



**Politecnico
di Torino**

Politecnico di Torino

Corso di Laurea Magistrale in Ingegneria dei Materiali

A.a. 2022/2023

Sessione di Laurea Ottobre 2023

Improved efficiency of organic solar cells based on crystals oriented by the friction transfer method

Relatori:

Sangermano Marco
Yamao Takeshi
Inada Yuhi

Candidati:

Roberto Petrasso

Abstract:

For organic photovoltaic devices (OPVDs), controlling the molecular orientation is crucial for obtaining high efficiency. In the present research, highly oriented crystalline films of thiophene-phenylene co-oligomer (TPCO) material were grown on a thin orientation template of friction-transferred polythiophene (PT). To further increase the orientation, thermal treatments were performed to induce recrystallisation of the TPCO layer. XRD, SEM, and polarised absorption analyses confirmed a high level of orientation, demonstrating that the annealing could further enhance the orientation. Moreover, the annealed samples exhibited a promising block-like crystal structure, which has the potential for creating an interpenetrated bulk heterojunction. Based on this structure, OPVDs were fabricated having TPCO molecules and C₇₀ as the organic semiconductors, and, subsequently, their electrical properties were evaluated. However, the results indicated a decrease in the power conversion efficiency (PCE) of the devices when friction transfer and annealing were performed. Investigations of the causes and possible solutions were proposed in order to find a way to increase the PCE.

Index of contents

Abstract	2
Introduction	4
1. Chapter one - Background information	
1.1. Organic semiconductors	5
1.2. Thiophene-Phenylene Co-Oligomers (TPCOs)	5
1.3. Organic photovoltaic mechanisms	5
1.4. OPVDs characterisation	8
2. Chapter two - Friction-transferred thin films	
2.1. Different method for molecular orientation	10
2.2. Experimental	11
2.3. Results and Discussion	13
3. Chapter three – Oriented films of TPCO	
3.1. Experimental	16
3.2. Results and Discussion	16
4. Chapter four – Thermal treatment	
4.1. Enhancing crystallinity	23
4.2. Experimental	23
4.3. Results and Discussion	24
5. Chapter five – Production of OPV devices	
5.1. Device structure	31
5.2. Experimental	32
5.3. Results and Discussion	34
5.4. New experimental phase	41
5.5. New results and Discussion	42
Conclusions and future perspectives	47
Acknowledgments	48
References	49

Introduction

Every year, the top of Earth's atmosphere receives an average amount of solar power equal to 1361 W/m². When passing through and reaching the surface, this energy value gets attenuated to approximately 1050 W/m² at sea level (when the sun is at the Zenit during a cloudless day) ^[1]. This value is still subject to various corrections because of radiation re-emittance, absorption, and angle of the surface. If we do not consider clouds, the average daily solar irradiance is 6 kWh/m². This tremendous amount of power is the most easily found source of alternative energy. While, on the one hand, inorganic photovoltaic is a well-established means for harvesting such energy, on the other hand, organic photovoltaic devices (OPVDs) represent a promising alternative that is yet to be fully spread throughout the world. Flexibility, lightweight, better disposability, and cost efficiency are the factors leading the research in the organic field. Moreover, organic molecules allow a fine-tuning of the absorption band by functionalising the polymeric chains. The most challenging task for organic devices is overcoming the comparison in efficiency and lifetime with the inorganic counterpart. While Si-based devices can easily reach more than 20% PCE and have a lifespan of over a decade, OPVDs have a relatively short life, in which they struggle to get values of PCE higher than 10%. Only in recent years novel devices with a PCE of 16.5% ^[2] have been developed, but it is also well known that, when combined into a large size module, the overall efficiency decreases by almost 5% ^[3]. Now that the great potential of organic photovoltaics has been widely recognised, the research has made significant advances in OPVs towards high PCE, long-lasting devices, and large-area processing.

When fabricating electronic devices based on organic thin films, generally, the choice of the material is not the only parameter influencing the final properties of the device. The morphology of the film plays a role as important as one of the intrinsic characteristics of the semiconductor. This is the reason why research in this field is not limited just to molecular engineering of the semiconductors but also focuses on both the process and the ways to optimise the structure of the device. Parameters such as crystallinity, thickness, anisotropy, and so on can greatly influence the final properties. If the organic semiconductors are conjugated polymers, then anisotropy becomes a key factor for enhancing the characteristics of those devices.

In this study, in order to obtain a highly anisotropic film, the friction transfer technique was chosen as the molecular orientation method. The friction transfer (FT) is a simple and cost-effective orientation method that does not require solvents or a vacuum. The thin films created by FT are highly oriented and can work as orientation templates: if additional material is deposited on top of the FT layer, this will get oriented as well ^[4-6]. Since it does not require solvents, FT can be used also for the deposition of insoluble materials such as polythiophene (PT), a π -conjugated polymer. In the present research, thin films of oriented PT were deposited with the FT method. These films were used to realise an orientation template for the subsequent deposition of T4P, an organic semiconductor belonging to the thiophene-phenylene co-oligomers (TPCOs) family. The resulting morphology has been studied, and thermal treatments were performed in order to enhance the crystallinity and the orientation of the organic materials. Organic photovoltaic devices based on this structure have been realised, and their properties have been analysed.

Chapter 1 – Background information

1.1. Organic semiconductors

Usually, polymers are insulator materials, non-capable of conducting electricity. Organic materials showing charge transport mechanisms are typically conjugated polymers, materials in which there is an overlapping of p-orbitals across an adjacent σ -bond. In the conjugated region where the two orbitals overlap, π electrons are delocalized and do not belong to a single bond or atom anymore but are, instead, shared by all the aligned and adjacent p-orbitals. If the conjugated system is not localised on a single bond, but throughout the entire molecular chain, then the electrons become delocalised along the entire molecule, creating an organic semiconductor.

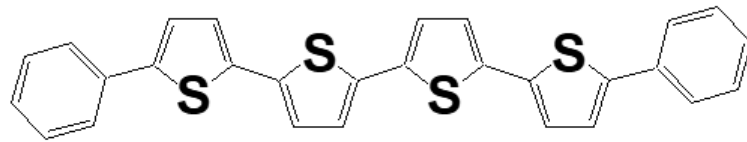
When talking about standard inorganic semiconductors, the energy gap E_g , defined as the difference between the energies of conduction and valence bands, is the main property to consider. A semiconductor can absorb only radiations with an energy equal to or greater than its E_g . For photovoltaic applications, it is necessary to narrow the distance between the two bands in order to have a broader absorption spectrum. When talking about organic semiconductors, instead, the two bands are substituted by their equivalents: LUMO (lowest unoccupied molecular orbital) and HOMO (highest occupied molecular orbital). The energetic difference between HOMO and LUMO has the same role for organic semiconductors as the E_g for inorganic semiconductors. While inorganic semiconductors have significant issues in creating materials with a specific bandgap, organic semiconductors present relatively easy solutions for fine-tuning the absorption and emission spectra thanks to different molecular designs, synthesis methods, and processing ^[7].

1.2. Thiophene-Phenylene Co-Oligomers (TPCOs)

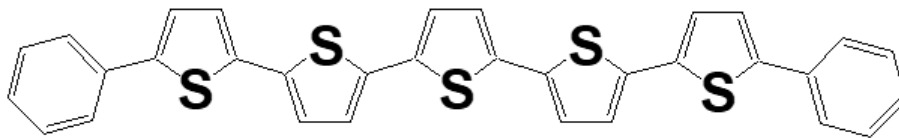
TPCOs constitute a family of low molecular weight organic semiconductors. Their molecules are composed of a one-dimensional chain of thiophene and phenylene rings. A few examples are shown in Figure 1.2.1. The symmetry and the order of the rings define different opto-electronic properties specific to each molecule. TPCOs can be synthesized with high precision and very low impurities, so it is possible to obtain a material with arbitrary electronic structures. Their anisotropic structure allows for easy orientation and crystallization, ideally enhancing even more the electronic properties. As for many other organic semiconductors, TPCOs are a p-type semiconductor that uses holes as the main charge carrier.

1.3. Organic photovoltaic mechanisms

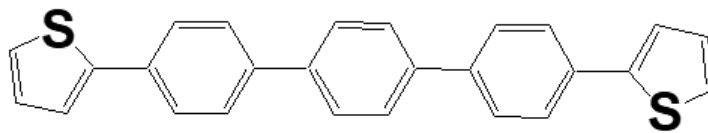
The typical structure of an OPVD is based on a p-n heterojunction of two types of organic semiconductors as shown in Figure 1.3.1. At the active layer of the two semiconductors light absorption takes place. The photogenerated charge gets separated by the respective electrode giving electricity if the device is connected to a circuit. The process by which an OPVD transforms light into current can be divided into seven different steps ^[8]:



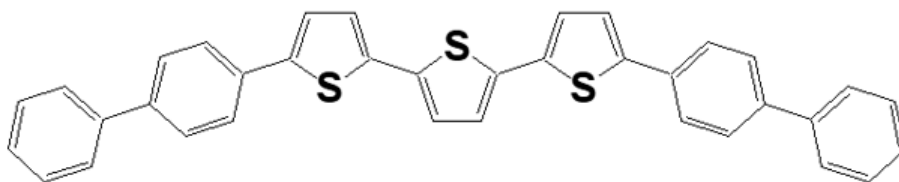
5,5'''-Diphenyl-2,2':5',2'':5'',2'''-quaterthiophene (P4T)



5,5''''-Diphenyl-2,2':5',2'':5'',2''':5''''-quinquethiophene (P5T)



4,4''-Di(2-thienyl)-1,1':4,1''-terphenyl (T3P)



5,5''-Bis(4-biphenyl)-2,2':5',2''-terthiophene (BP3T)

Figure 1.2.1. Examples of TPCO molecules

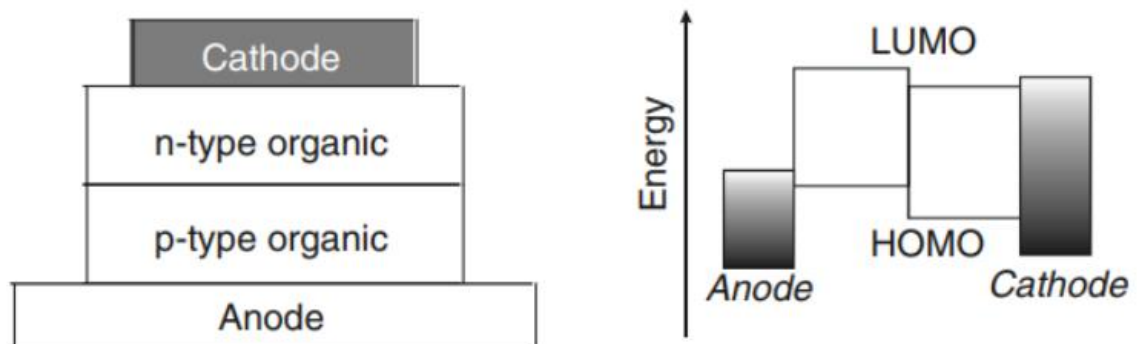


Figure 1.3.1. Schematic diagram of a heterojunction OPVD

- **Incoupling of the photon:** when the photon reaches the device, it is essential to have an interface as transparent to light as possible. In order to reduce efficiency losses, it is in fact crucial to reduce the reflectance of the device-air interface. If reflection does not occur, the photon can then be absorbed.
- **Photon absorption:** as explained in the previous paragraph, if the photon has an energy equal to or greater than the band gap of the semiconductor, then it can be absorbed. The eventual difference in energy will be converted into thermal energy.
- **Exciton formation:** after optical absorption occurs, an exciton is generated. It consists of an electron-hole pair coupled together into a neutral particle by Coulomb forces. Not all the absorbed photons are converted into excitons.
- **Exciton migration:** after being generated, the exciton moves with a Brownian motion through the volume of the material. Excitons have a limited lifetime before the two charges recombine. The average lifetime is in the order of pico- to nanoseconds, leading to a diffusive distance of approximately 5 – 10 nm. The natural decay of the exciton can be thermal, vibronic, or radiative, leading, in any case, to a loss in efficiency.
- **Exciton dissociation:** in order to obtain electrical energy from the decay of the exciton, it is necessary to separate the two charges (electron and hole) into two free carriers. The energy required to dissociate the exciton is typically between 0.5 - 1.5 eV, which is much higher than the thermal energy at room temperature ^[9]. The most efficient way of doing it is by using the difference in potential energy of the p-n junction. The excitons that during their random motion reach the interface between the two semiconductors will dissociate into an electron and a hole. Considering the limited lifetime (and thus diffusion length) of the excitons, it is clear that only the excitons generated close to the junction interface will be able to generate free charges; all the others will decay, with a consequent reduction in efficiency. Reducing the thickness of the semiconductor layer will lead to a proportional decrease in absorbance, so the best solution is to fabricate bulk heterojunctions in which the interfacial area between the two sides is maximized. The optimal condition would be an interpenetrated structure of the two semiconductors ^[9-12] such as the one shown in Figure 1.3.2
- **Charge transport:** to get the actual photocurrent, the free charges must be allowed to reach the electrodes. During their transport the carriers can be subjected to recombination at the interface or get trapped inside defect points. Both cases lead to a loss in efficiency. To increase the probability of the charge reaching the electrode, one should reduce the thickness of the semiconductive layer, but this will, as mentioned above, reduce the overall absorbance.
- **Charge collection at the electrodes:** even if an electron or a hole is present close to an electrode, it is not sure whether they will pass into the outer circuit. The probability associated with all the

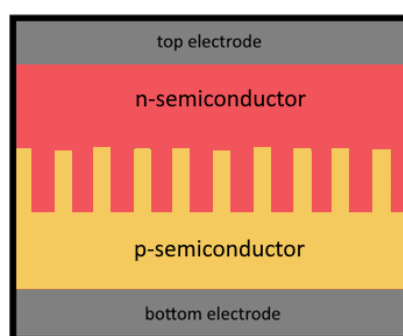


Figure 1.3.2. Schematic illustration of an optimal interpenetrated heterojunction

barrier penetration mechanisms involved at the interfaces towards the metallic surfaces is a function of geometry, topology, and interface formation.

The main photophysical processes of photocurrent generation and efficiency losses described here are also summarised in Figure 1.3.3.

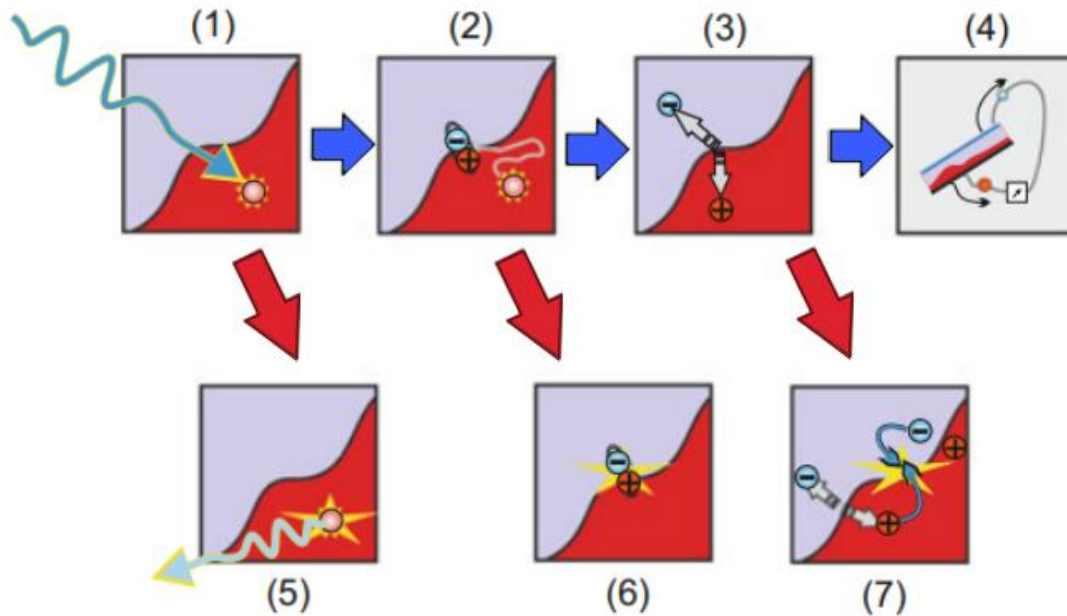


Figure 1.3.3. Schematic representation of the photophysical processes inside an OPVD. The blue arrows indicate the succession of events that lead to photocurrent generation, and the red arrows indicate the possible events that lead to energy dispersion and efficiency losses.

- (1) Photon absorption and exciton generation. (2) Migration of the exciton and dissociation into free opposite charges when reaching the interface. (3) Charge transport towards the electrodes. (4) Charge collection at the electrodes and photocurrent generation inside the associated circuit. (5) radiative decaying of the exciton. (6) Free charges recombination. (7) Non-geminate recombination of the free charges

1.4. OPVDs characterisation

The performances of photovoltaic devices are described by a current-voltage diagram like the one shown in Figure 1.4.1. The main properties are the short circuit current J_{sc} , the open circuit voltage V_{oc} , and the maximum power P_{max} . J_{sc} is proportional to the amount of exciton the device is capable of separating, V_{oc} is related to the difference between HOMO of the p-region and LUMO of the n-region. Their product defines the potential power of the device. P_{max} is the maximum value of the product of current and voltage when the device is connected to a circuit. These current and voltage are denoted as J_{max} and V_{max} , respectively. The fill factor ff can be then defined as:

$$ff = \frac{J_{max} \cdot V_{max}}{J_{sc} \cdot V_{oc}} = \frac{P_{max}}{J_{sc} \cdot V_{oc}}$$

This basically corresponds to the ratio between the blue and red area in Figure 1.4.1. The main parameter is the power conversion efficiency (PCE – η_e), which is calculated as the ratio between

the maximum electrical power generated (P_{max}) and the incident optical power (P_o):

$$\eta_e = \frac{P_{max}}{P_o} = \frac{J_{max} \cdot V_{max}}{P_o}$$

The value of PCE defines the capability of the device of converting the solar radiation power into electrical power. Lastly, PCE allows to calculate the external quantum efficiency (EQE), defined as the number of electrons generated per incident photon:

$$EQE = \frac{\eta_e}{\eta_{ph}} = \frac{I_{sc} \cdot hc}{P_o \cdot \lambda e}$$

where h is Planck's constant, c is the speed of light, λ is the incident wavelength and e is the electrical charge. This last parameter is used to evaluate the photoconversion efficiency of the device. From a theoretical point of view, the EQE is linked to the PCE, having η_e equal to the integral of EQE over the entire solar spectra, and multiplied by the monochromatic power efficiency. On a practical point of view, though, this equation fails to calculate the PCE because the fill factor depends on the wavelength, and the device efficiency is often inversely proportional to the light intensity^[13].

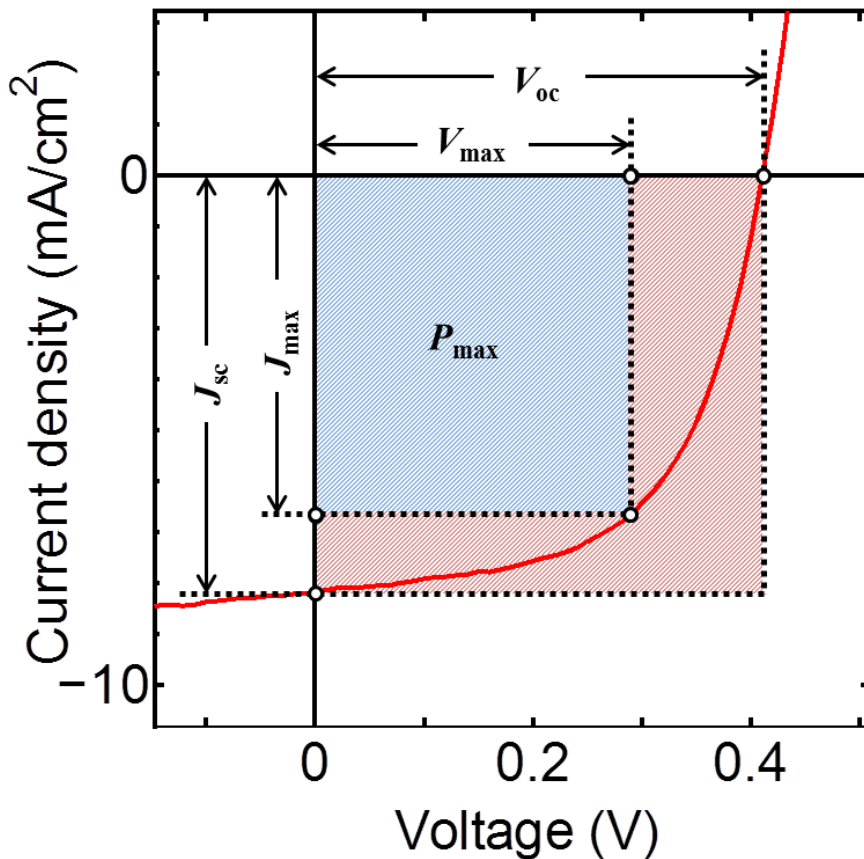


Figure 1.4.1. Current voltage response of a photovoltaic device under illumination

Chapter 2 – Friction-transferred thin films

2.1. Different methods for molecular orientation

As explained in the previous chapter, controlling the molecular orientation of the organic layer is essential for maximizing efficiency and for channelling the charge transport along a single direction in the electronic devices based on such films. When building OFETs, this direction should be the one parallel to the substrate connecting drain and source. In contrast, when building OPVDs, this direction should be the one perpendicular to the substrate, connecting top and bottom electrodes through the layered structure of the device. There are several different methods for achieving molecular orientation of conjugated polymers, mainly mechanical (stretching and rubbing methods) or solvent-assisted (liquid-crystal self-organization ^[14] or the Langmuir-Blodgett method ^[15]). However, the above-mentioned methods, are not completely suited for creating opto-electronic devices. For example, the Langmuir-Blodgett method can be used only for depositing amphiphilic materials, and the resulting films usually suffer from several defects such as aggregations. The rubbing method, instead, increases the roughness of the surface, also increasing the chances of having short circuits.

Among the mechanical methods, there is the friction transfer (FT) technique. This process was first discovered by Makinson and Tabor in 1964 ^[16], when it was used for the orientation of poly(tetrafluoroethylene) (PTFE). The FT method is a simple and cost-effective technique that allows to obtain highly oriented films of material without the use of vacuum, controlled atmospheres, or solvents. As illustrated in Figure 2.1.1, the process consists in squeezing a polymer onto a hot, moving substrate. The result will be a film of material aligned in the same direction as the one of the FT. The combination of temperature, pressure, and speed defines the thickness of the film.

The true potential of the FT method, though, was later discovered in 1991 by Wittmann and Smith ^[17], who used the friction-transferred PTFE of Makinson and Tabor as an orientation template for the deposition of other materials. The FT layer can induce its orientation on the materials that grow on top of it, regardless of whether it is from melt, solution, or vapour phases. This characteristic in particular allows for a great versatility in terms of chemical and physical properties of the deposited materials. For instance, the spin coating, one of the most common deposition methods, does not induce any orientation, but, since the FT allows to deposit also insoluble materials, it is possible to perform a spin coating on top of a friction-transferred layer of an insoluble material: the bottom layer, being insoluble, will not be altered, while, on top of it, the soluble spin-coated material will get oriented.

Thanks to its simplicity and versatility, the FT method has attracted many researchers, and many materials combinations have been studied. The orientation of TPCOs by the FT method, though, has not been fully developed, and the properties of electrical devices such as OLEDs and OPVDs based on this structure have not been studied yet. In this research, in order to get an oriented layer of TPCOs, a highly oriented thin film of polythiophene (PT) has been created by the FT method. PT is a conjugated polymer. Since the hypothetical future device will have the FT layer set between the bottom electrode and the semiconductor, it is important for the friction-transferred material to be able to conduct electricity, otherwise the FT layer would also act as an insulator, preventing the device from working. This is the reason why PTFE, the most common FT material, has not been used.

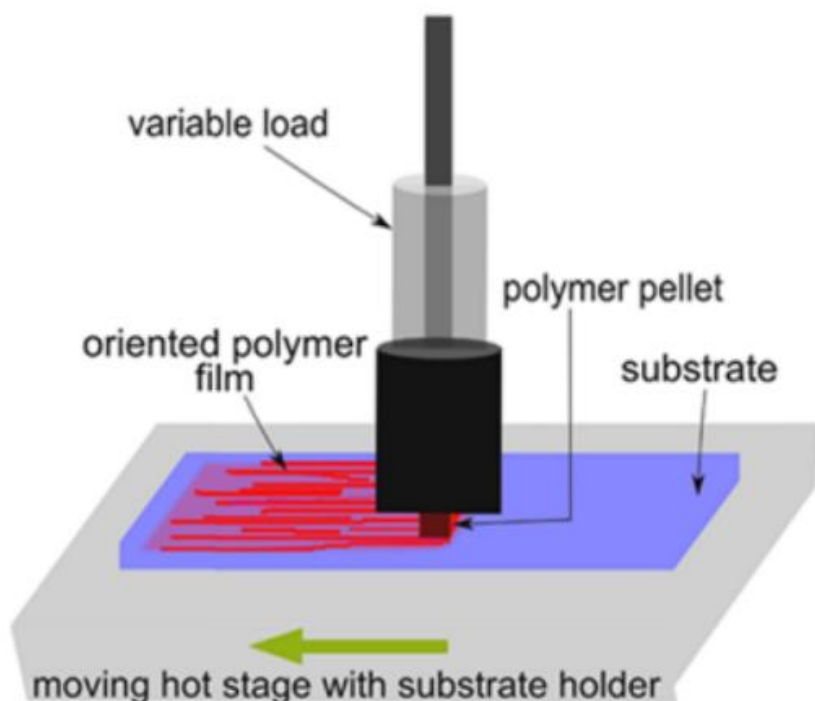
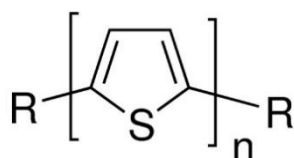


Figure 2.1.1. Schematic illustration of the friction transfer technique

2.2. Experimental

Powders of PT (Poly(thiophene-2,5-diyl), Bromine terminated), were purchased by Sigma-Aldrich and used without further purification. Its chemical structure is shown in Figure 2.2.1. PT powders were compressed into a pellet (diameter $\phi = 1.3$ mm) using a hydraulic press by applying a pressure of 5 tons for 40 minutes under vacuum. The pellet obtained this way was then cut with a razor blade and the cutting surface was polished using abrasive SiC paper (P400 – P1000) to obtain a smooth, flat interface. During the experiments, it was found that low roughness and smoothness of the contact surface between the pellet and the substrate are important factors to achieve an optimal deposition. In addition to that, the two surfaces should be as parallel as possible. Figure 2.2.2 explains in a schematically the effect of the pellet shape on the quality of the deposition. The pellet was not cut into a semi-circular shape in order to distribute the load on a wider area. The PT pellet was easily broken during the process when it had a semi-circular shape, resulting in a non-optimal deposition. The shape used drastically reduced the probability of having the pellet break during the deposition.



R = H or Br

Figure 2.2.1. Chemical structure of polythiophene (PT)

PT was deposited by the FT method onto quartz substrates and mono-Si substrate covered with a 100-nm thick oxide layer. Those substrates were cleaned sequentially in acetone, isopropanol, ethanol, and distilled water under ultrasonication for 10 minutes each. They were then dried by nitrogen gas blowing and finally exposed for 10 minutes to a UV-Ozone treatment.

The FT process was carried out heating the substrates at 250 °C, applying a pressure of 20 kgf/cm² (≈ 2 MPa/cm²), with a drawing speed of 1000 mm/min. Based on the available literature, these are the best conditions for the FT deposition of PT [18-20]. The orientation of the PT layer was evaluated through polarised microscopy, and polarised absorption spectra analyses.

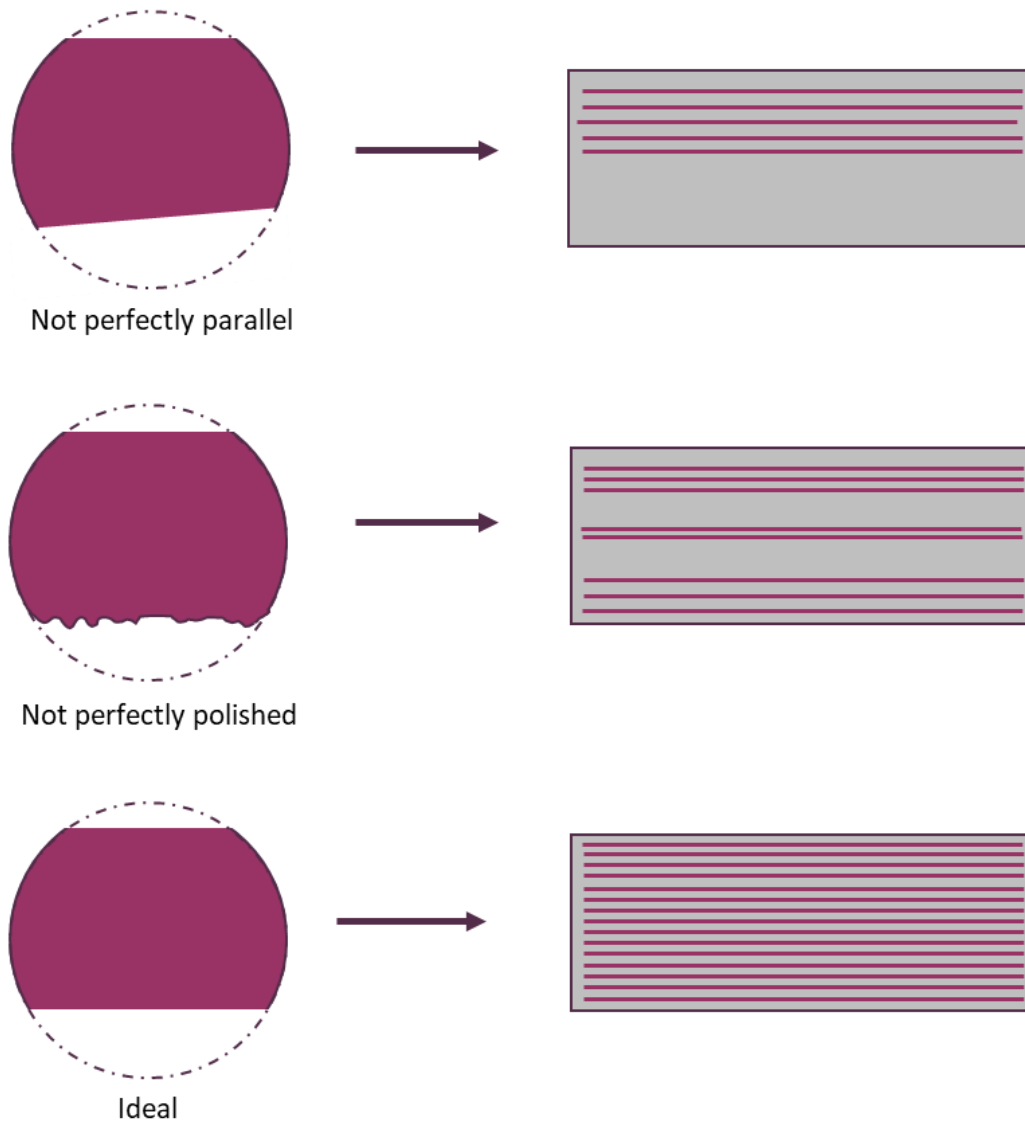


Figure 2.2.2. Schematic illustration of the effect of the pellet surface quality on the friction transfer deposition

2.3. Results and Discussion

Polarising microscope: PT films deposited on Si/SiO₂ substrates were observed with a polarising microscope under the crossed-Nicols condition. In this condition, the two polarisers are placed perpendicular to each other between the lens and the sample. If the sample has birefringence properties, that is having an anisotropic refractive index, then its image will change depending on the angle between the sample and the polarisers. By rotating the sample on its stage by 45°, it will alternate from the extinction position to the diagonal position. In the former, no light is passing, and the image is always dark. In the latter, birefringent materials will show bright images, whereas isotropic materials will still have dark images.

When the friction-transferred PT was observed under crossed-Nicols in the diagonal position, the film was bright (Figure 2.3.1 (b)), indicating a good molecular orientation. The image shows a wavy structure of alternating peaks and valleys, creating stripes oriented along the FT direction. When observed without polarisers (Figure 2.3.1 (a)), the PT film was so thin that it was hardly visible, and only the broader peaks could be seen.

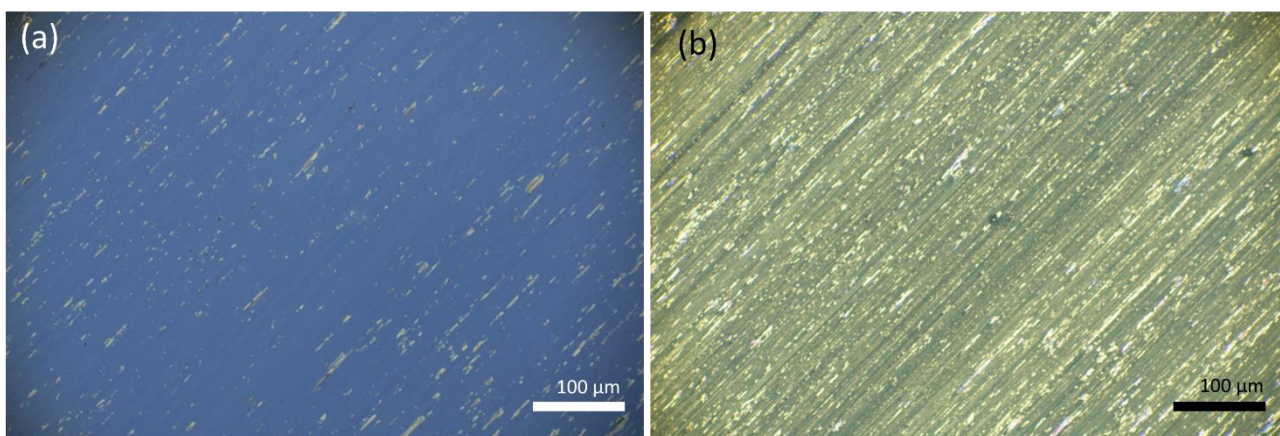


Figure 2.3.1. Friction transferred PT film micrographies obtained with a polarising microscope with a 10x magnifying lens under (a) normal conditions and (b) crossed-Nicols condition. The friction transfer direction is from top-right corner to bottom-left corner

Thin film step difference meter: the thickness of the PT film was analysed by a stylus-type step difference meter. The results (Figure 2.3.2) confirm the wavy structure seen under the microscope: the peaks are 5 – 6 nm thick, and the valleys are around 2 nm thick. The average thickness of the film was below 5 nm. Some major peaks were observed during the analysis, reaching 35 to 50 nm. They can be associated with small aggregates of PT caused by irregular delamination of the pellet. These types of aggregates appear frequently in the friction transfer layer. They constitute most of the broad peaks observed in Figure 2.3.1. (a), and, by what has been observed during the experimental phase, it was impossible to avoid their formation.

Polarised absorption spectra: PT films deposited on quartz substrates were used for UV-vis polarised absorption spectra analysis; the results are shown in Figure 2.3.3. The measurement was conducted varying the wavelength of the polarised light from 300 to 800 nm. When the light was polarised parallel to the friction transfer direction, the spectra showed absorption peaks at 516, 557, and 607 nm. When the light was polarised perpendicular to the friction transfer direction, no clear peaks could be seen, just a flat, low intensity, absorption band. The high level of noise observed for

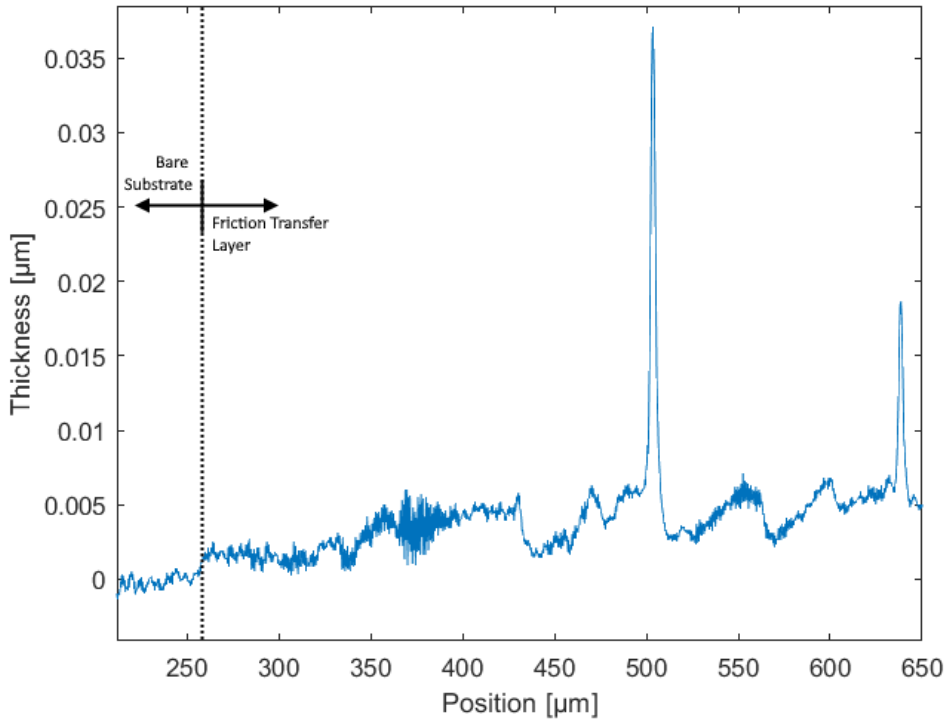


Figure 2.3.2. Step difference thickness analysis of the friction-transferred PT layer

low wavelengths is caused by the measuring instrument. The overall shape of the obtained spectra, with a clear difference in the absorbance depending on the polarization direction, proves the orientation of the PT layer. The results, though, do not reproduce the same level of orientation obtained by other researchers^[18-20]. The dichroic ratio (DR) and the order factor (F) were calculated as:

$$DR = \frac{A_{//}}{A_{\perp}}$$

$$F = \frac{DR - 1}{DR + 2}$$

where $A_{//}$ and A_{\perp} are the integrated absorbances between 300 and 800 nm of the light polarised parallel and perpendicular to the FT direction respectively. The analysed samples had an average value of $DR = 1.6$. The resulting order factor has a mean value of 0.19. The order factor is a number that ranges from 0 to 1, where 0 means no orientation and 1 means complete uniaxial orientation. Such low values of F are not completely coherent with the expected highly oriented structure. The reasons behind these values could be multiple: first of all, the PT layer is very thin, so the overall absorbance of light is low as well and hardly detectable by the machine used. Such low thickness also contributed to increasing the noise registered at lower wavelengths. Moreover, the experimental setup, due to the necessity of manually aligning sample and polariser, is also easily subjected to artificial errors. Any small misalignment leads to different values of absorbance compared to the real ones. To be more precise, differences in the alignment lower the value of $A_{//}$ and increase the values of A_{\perp} , leading to an overall reduction of DR . Taking into account all these possible errors, it is still possible to confirm the orientation of the friction-transferred PT.

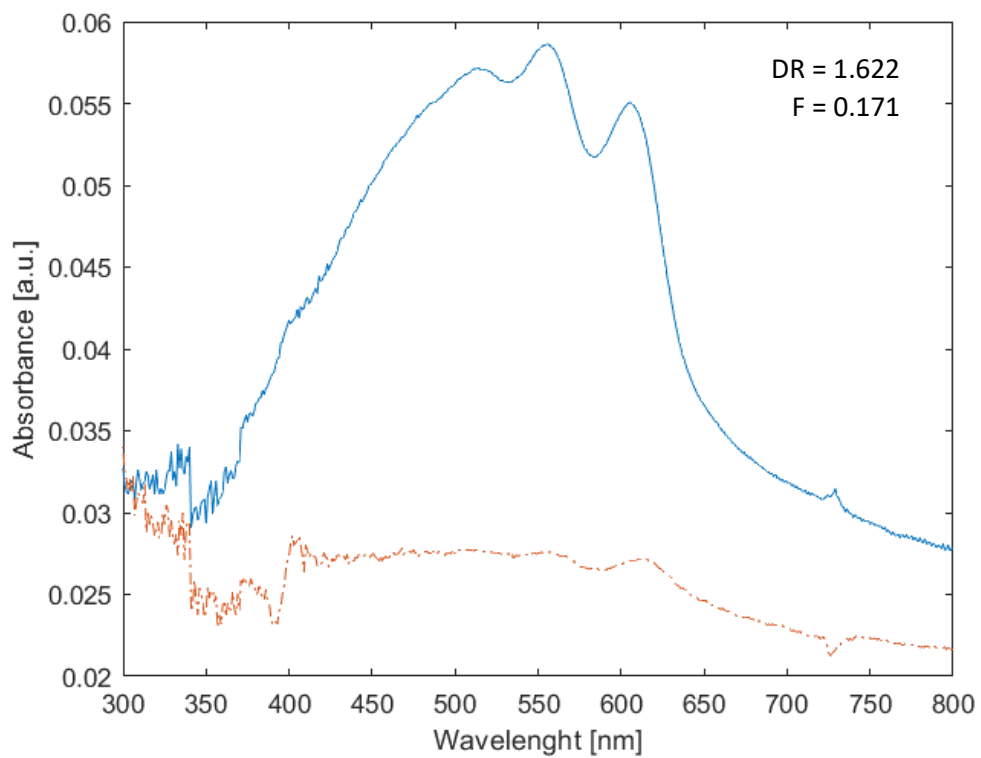


Figure 2.3.3. Polarized absorption spectra of the friction-transferred PT layer with light polarized parallel (blue line) and perpendicular (red dashed line) to the FT direction

Chapter 3 – Oriented films of TPCO

3.1. Experimental

The TPCO molecule chosen for this research is 4,4''-di(2-Thienyl)-1,1':4',1'':4'',1'''-quaterphenyl (T4P), chemical structure shown in Figure 3.1.1. The organic semiconductor has been deposited on top of the PT friction transfer layer on both the samples realized on quartz and Si/SiO₂ substrates. In order to have a comparison, T4P has been deposited also on clean quartz and Si/SiO₂ substrates.

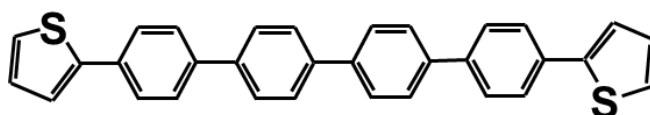


Figure 3.1.1. Chemical structure of T4P

Deposition of T4P was performed by organic vapour deposition under vacuum at pressures below $5 \cdot 10^{-3}$ Pa, with a deposition rate between 0.01 – 0.02 nm/s. The thickness of the T4P layer was 80 nm. The morphology and orientation of this layer have been analysed by polarised microscopy, polarised absorption spectra, and X-ray diffraction (XRD) analyses.

3.2. Results and Discussion

Polarising microscope: when observed under normal conditions (Figure 3.2.1 (a) and (c)), the samples show a clear superficial pattern which is analogue to the one observed with just the PT layer. Contrarily to the PT layer, the T4P layer can be clearly seen even with naked eye. When observed under the crossed-Nicols condition and tilted by 45° compared to the polarisers (diagonal position - Figure 3.2.1 (b) and (d)), the samples exhibited highly bright images in which the oriented pattern was clearly visible. These images confirmed the good orientation of the TPCO layer and thus provided a qualitative demonstration of the orientation capabilities of the FT method. On the other hand, the images of the T4P layer deposited on clean substrates did not show any sign of orientation: their images were always dark, both in the extinction and in the diagonal position.

Polarised absorption spectra: new spectra analyses were conducted after the deposition of T4P on the samples with quartz substrates. Their results are shown in Figure 3.2.2. Compared to the previous data collected, the new spectra show absorption values much greater than what was measured for the sole layer of PT. The presence of the TPCO layer causes a change in the shape of the spectra, showing a wide absorption peak between 300 – 450 nm. The sharp step that can be observed between 300 – 350 nm is caused by light scattering defects. This problem cannot be avoided because it is intrinsic to the machine used. Since the step is much more evident when the light is polarized parallel to the FT direction, it is possible to assume that the scattering effect was much greater, and that the actual absorbance should have a non-flat peak with greater intensity than what was measured. Keeping this in mind, it is then necessary to use these data only in a quantitative way, because these errors will strongly affect the calculated DR and F. Since the intensity of the measuring error is much greater than what was observed in the previous analyses, it is believed that another

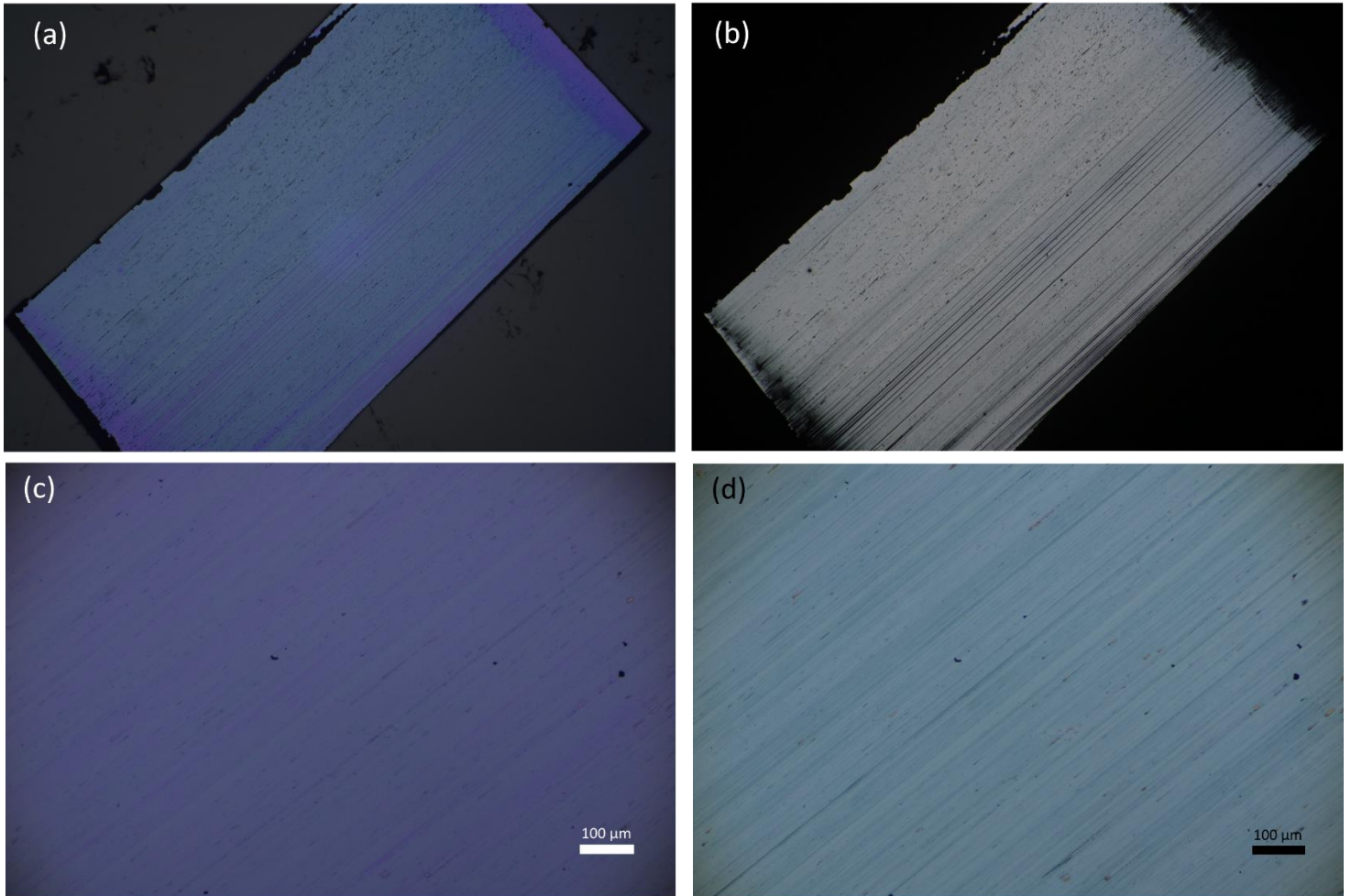


Figure 3.2.1. Polarising microscope images of the T4P layer deposited on top of the FT layer under (a,c) normal condition and (b,d) crossed-Nicols condition. Images (a,b) and (c,d) were taken with a 1x and 20x magnifying lens respectively. The friction transfer direction is from top-right corner to bottom-left corner

possible reason is that the presence of the polarizing lens is enhancing an already existing machine error. The machine used, in fact, is not supposed to work with polarized light. A polarising lens has been placed between the sample and the light source in order to obtain a polarised beam of light. The presence of these errors is forcing us, again, to use this data only in a quantitative way. The presence of dichroism confirms the orientation of T4P along the friction transfer direction. The true value of DR and F cannot be calculated, but, since they are all subjected to the same errors, it is still possible to compare them between each other. By doing this, it has been found that the orientation of T4P is directly proportional to the orientation of PT: the samples that had the highest values of DR and F for the PT layer, are now the ones with the highest values of DR and F for the TPCO layer. It is proven that the quality of the friction transfer layer does influence the orientation degree of the material deposited on top of it.

In the range between 500 – 600 nm it is possible to observe a less intense peak caused by the absorbance of PT. As can be seen in Figure 3.2.3, the parallel absorbance of this area is much greater than what was measured previously with just the friction-transferred PT layer, while the perpendicular absorbance is almost the same. These results hint at the possibility that the previous measurements did not have the expected results due to the low thickness of the PT layer. Considering, though, that the presence of 80 nm of T4P on top of the PT can increase the probability of light scattering, it is not possible to assume that the new results correspond to the actual value of

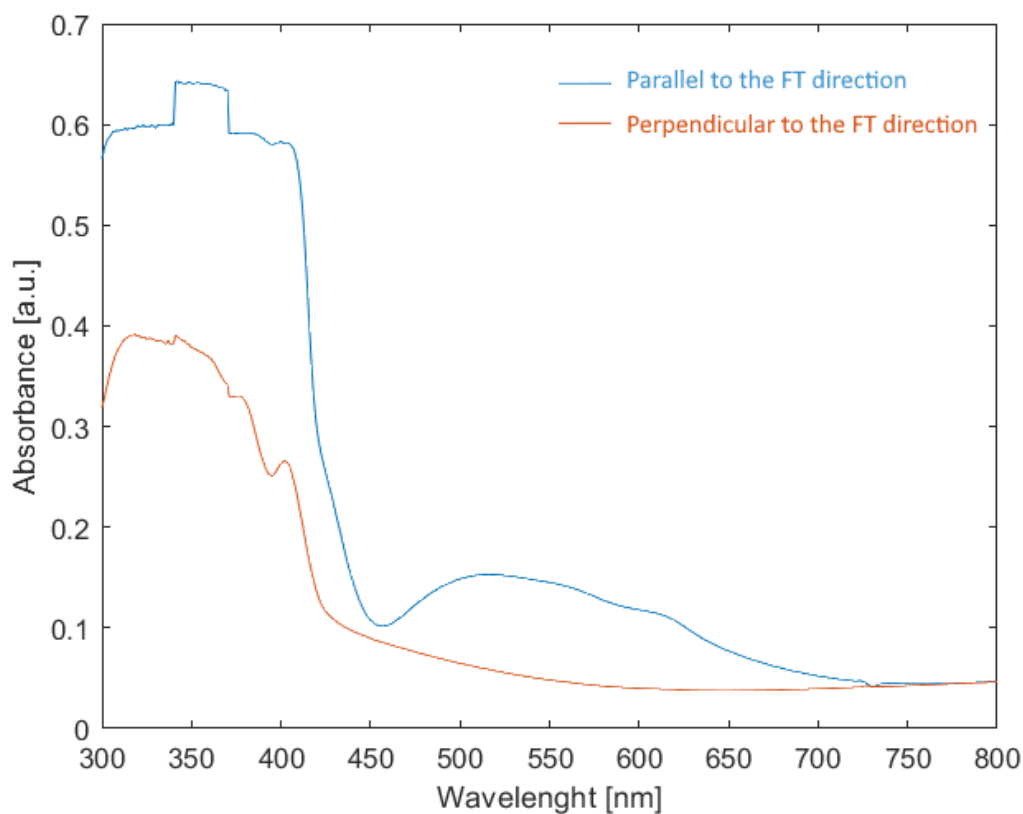


Figure 3.2.2. Polarized absorption spectra of the T4P layer deposited on top of a friction-transferred PT layer with light parallel (blue line) and perpendicular (red line) to the FT direction

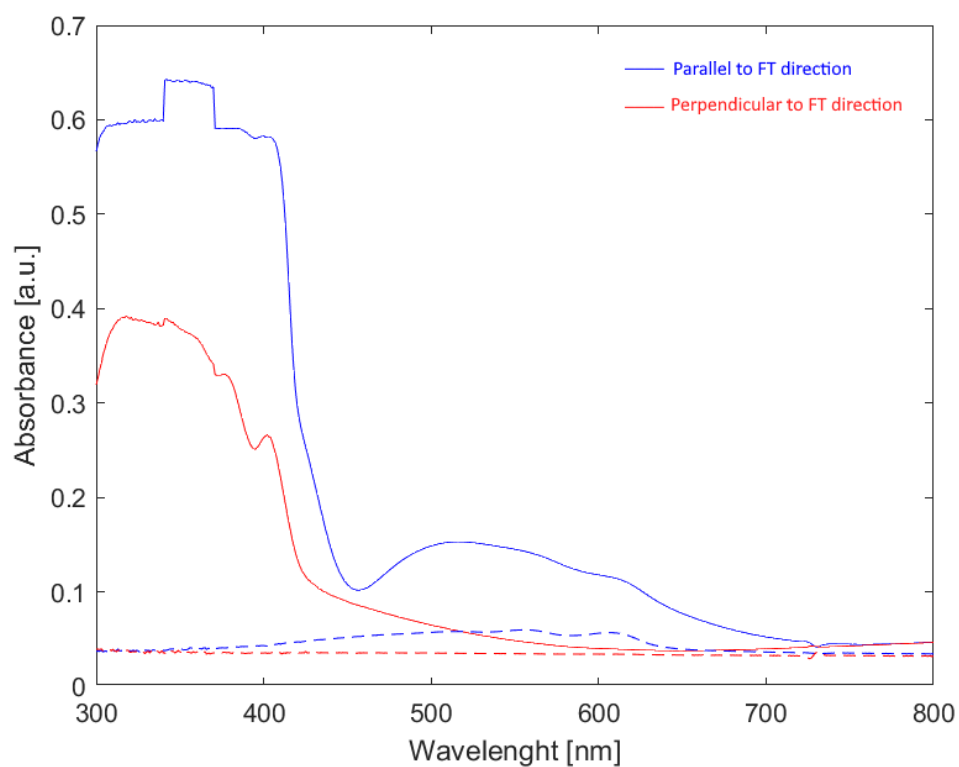


Figure 3.2.3. Comparison between the polarized absorption spectra of a friction-transferred PT layer (dashed lines) and of a T4P layer deposited on top of the FT layer (continuous lines)

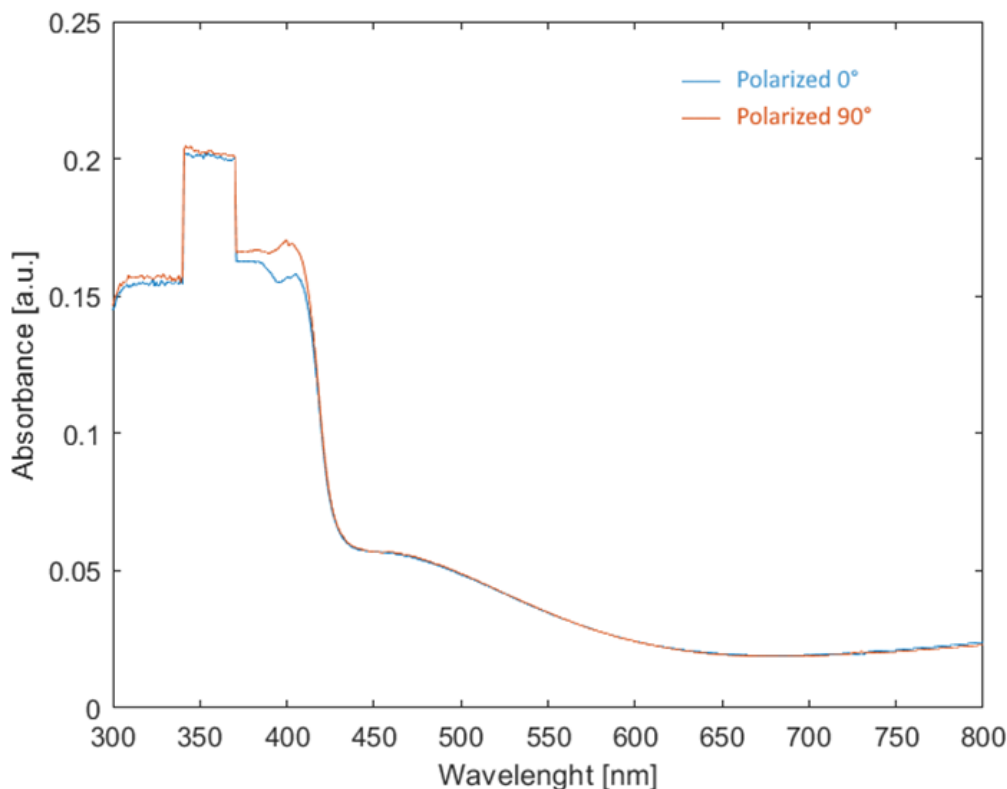


Figure 3.2.4. Polarized absorption spectra of T4P deposited on a clean quartz substrate (without FT)

absorbance of the PT layer. It is more correct to say that the actual absorbance of the friction-transferred PT is set at values between the continuous and the dashed line. Regardless of the actual value, this correction would always lead to an increase of DR and F, getting our results closer to the ones in the literature. Lastly, the samples without friction transfer were analysed. The results, shown in Figure 3.2.4, are coincident for both the polarisation directions, indicating, again, the lack of orientation.

XRD: diffraction analyses of X-rays were performed on the samples with Si/SiO₂ substrates. The angle 2θ varied between 2-30°, with a speed of 5°/min and step 0.010°. Results are reported in Figure 3.2.5 (a-d). All the obtained patterns show an amorphous peak between $2\theta = 17-30^\circ$. It is thought that this is the diffraction of the bottom oxide layer. It is possible that the TPCO layer could be thin enough to be able to measure the bottom SiO₂ layer diffraction.

The diffraction patterns of T4P deposited on the friction-transferred PT layer (Figure 3.2.5 (d)) show three main diffraction peaks, also highlighted in the graph, for values of $2\theta = 20.17^\circ$, 23.95° , 28.95° . Among these three, only the first and the second ones can be observed in the XRD pattern of T4P without the FT layer, while the third one is almost completely absent. The comparisons between the patterns with and without FT (Figure 3.2.5 (a-c)) shows that the presence of the PT layer enhances the intensity of each peak. The peak at $2\theta = 23.95^\circ$ is the one with the greatest increase. The amorphous peak gives a different base line for each sample. Regardless of the base intensity, samples with the FT layer always show a greater peak intensity than the ones without. This result highlights the role of the PT layer in the orientation of the polymeric material deposited on top of it.

For each peak the respective interplanar distance d was calculated using Bragg's diffraction law. The results are summarized in table 3.2.1. Since in the literature there is no crystal analysis of T4P, to understand the morphology of the TPCO layer XRD analysis of similar materials were used. TPCOs crystallites have usually a monoclinic structure and assume a packing scheme that is independent of the molecular shape and symmetry^[21]. In materials such as P6T and BP4T diffraction peaks can be found at similar values of 2θ , leading as well to similar values of d . For these TPCOs such values of d indicate a face-on orientation of the molecules, in which the main chain is lying horizontally on the substrate with the thiophene ring parallel to the surface.

Peak Number	2θ [deg]	d [nm]
1	20.17	0.4399
2	23.95	0.3712
3	28.95	0.3082

Table 3.2.1. XRD peaks position and relative value of interplanar distance

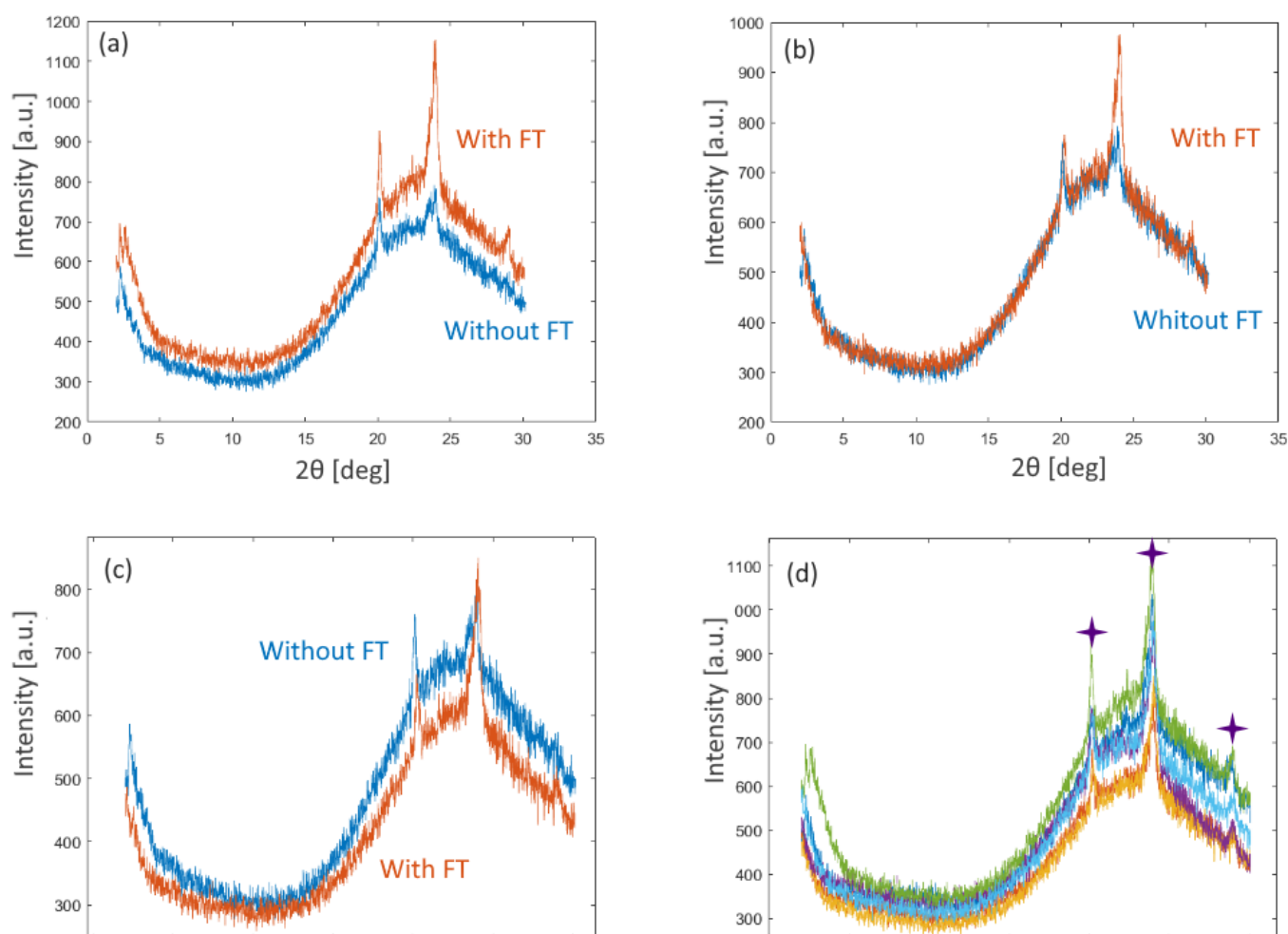


Figure 3.2.5. (a-c) Comparison between the XRD patterns of the T4P layer of samples with (red line) and without (blue line) the FT layer. (d) XRD pattern of the T4P layer deposited on friction-transferred PT, with highlighted peaks

In order to understand the nature of the broad amorphous peak, XRD of clean Si/SiO₂ substrates without any deposition were performed. The results (Figure 3.2.6) showed that the previous hypotheses were right, and the broad amorphous peak is in fact originated by the diffraction signal of the substrate. As demonstrated also by the comparison with the previously obtained patterns (Figure 3.2.7), this diffraction pattern constitutes the base line of the other XRD patterns obtained for the previous samples. A final comparison with data previously obtained in this laboratory showed that this diffraction pattern does not originate from the SiO₂ layer, but is, instead, the characteristic XRD pattern of monocrystalline Si(200) (Figure 3.2.8).

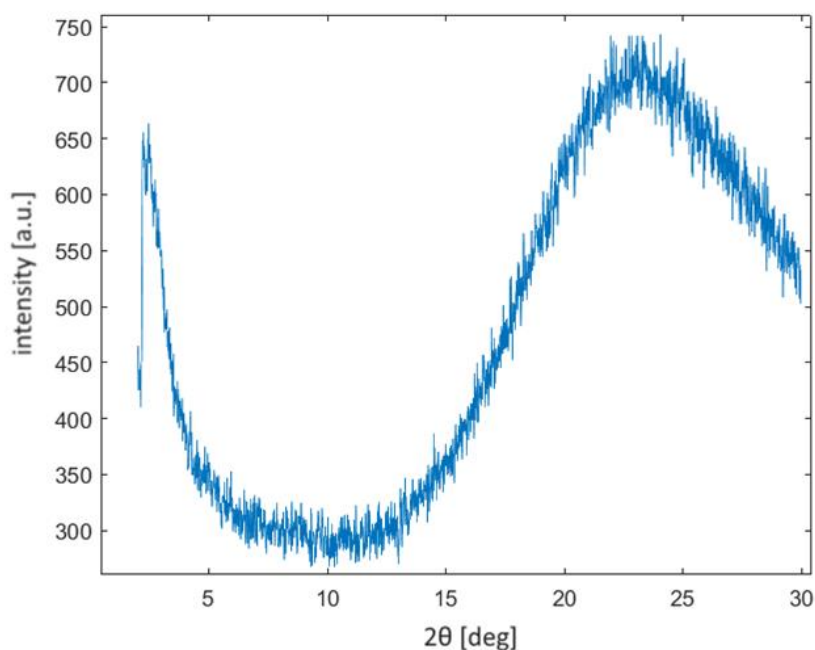


Figure 3.2.6. XRD pattern of a Si/ SiO₂ clean substrate

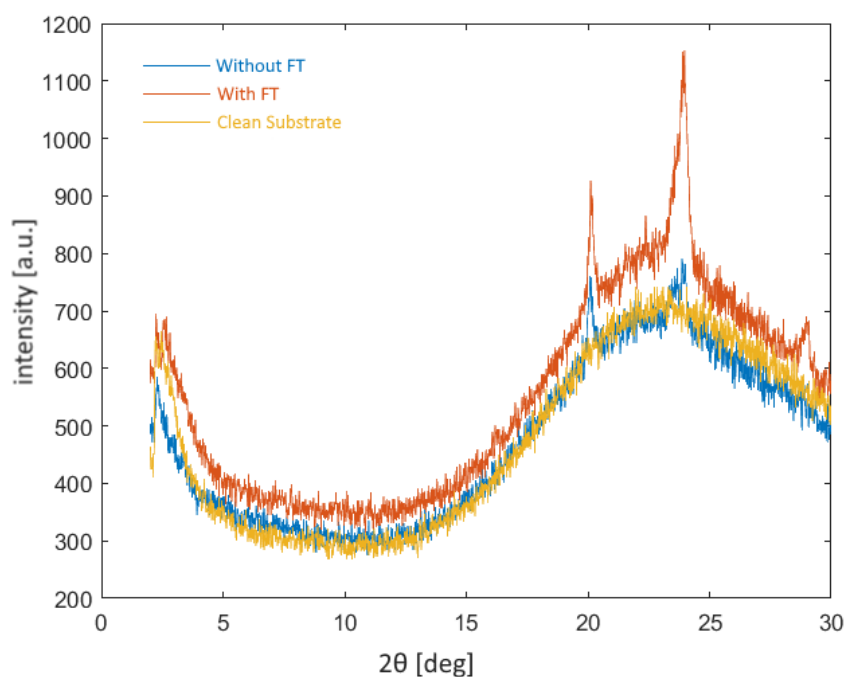


Figure 3.2.7. XRD patterns of a clean Si/ SiO₂ substrate (yellow line), a sample with FT (red line) and a sample without FT (blue line)

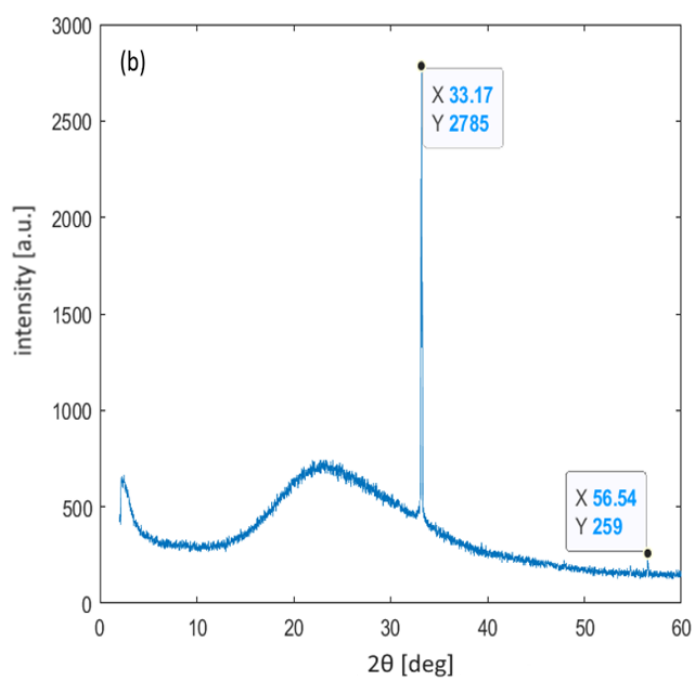
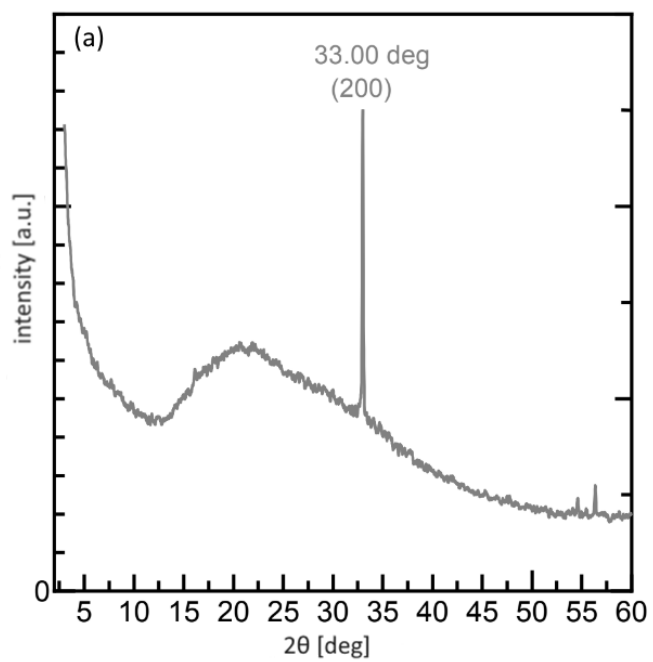


Figure 3.2.8. XRD pattern of (a) mono Si (200) and of (b) clean Si/ SiO₂ substrate

Chapter 4 – Thermal treatment

4.1. Enhancing crystallinity

As demonstrated by Inada et al. [22], even though the TPCO layer is highly oriented thanks to the FT layer, it is still desirable to enhance the crystallinity of the film. An increase in carrier mobility of the TPCO layer is observed after the annealing, leading to an increase in the efficiency of the devices based on those films. Kumari et al. [23] showed that the thermal treatment is also effective on the thin films produced by FT, causing an increase in the orientation, and a change in the main orientation of the molecular chains. With this process we are trying to achieve an even better degree of orientation and molecular order, so that the PCE of the final devices can be increased as well.

4.2. Experimental

In order to enhance the crystallinity of the TPCO layer, thermal treatments of both the samples realised on quartz and Si/SiO₂ substrates were performed. Both PT and T4P have high melting points, above 350 °C. Basing on the DTA data provided by the producer (Figure 4.2.1), T4P has a recrystallisation temperature around 320°C. This temperature would ensure the highest rate of crystallinity in the least time. The temperature for the thermal treatment, though, was chosen with regards to the glass transition temperature of PT, which is around 250 °C. If the FT layer undergoes a glass transition, then the high level of orientation of the upper TPCO layer would be partially lost. Thus, it was chosen to perform the annealing at 150 °C and 200 °C. The thermal treatment lasted for 1 hour and was performed under a nitrogen atmosphere created by blowing N₂ gas on the surface of the samples with a flow rate of 55 ml/s.

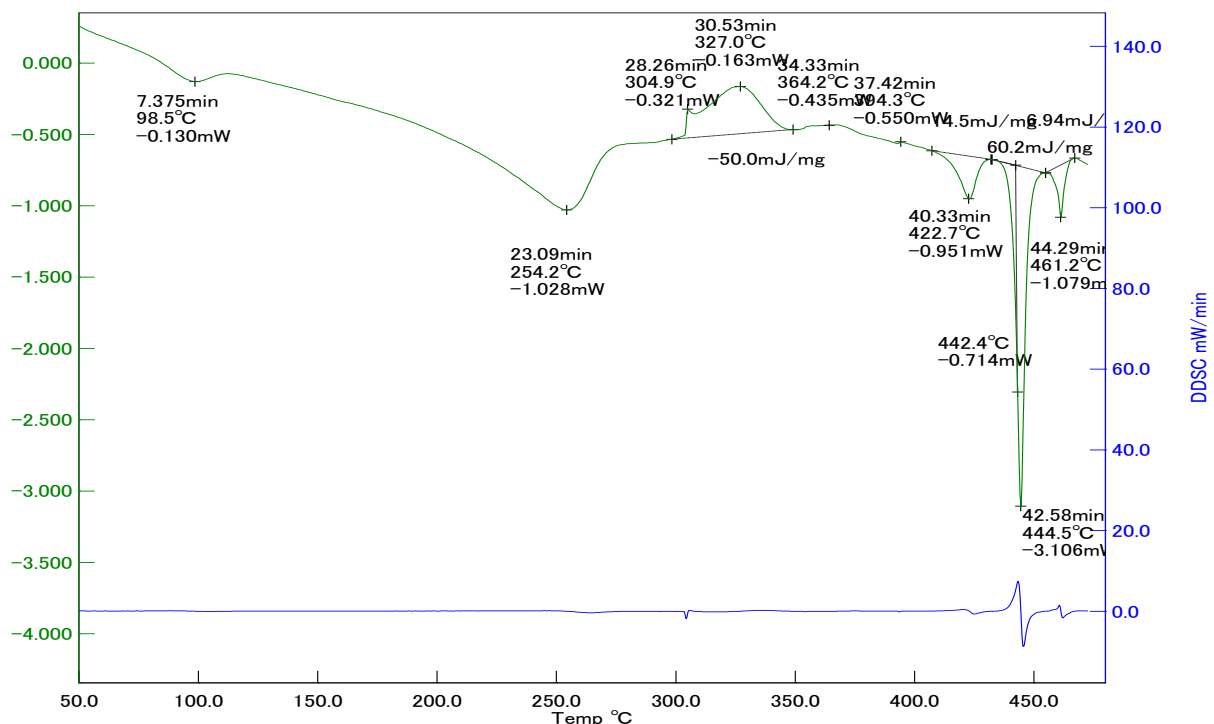


Figure 2.1. DSC and DDSC data of T4P

The annealed samples were observed with a polarising microscope. Then XRD and polarising absorption spectra analyses were performed again on the same samples to evaluate the changes brought by the thermal treatment, to confirm the increase in crystallinity, and to verify which temperature is the most suitable for the future production of electronic devices. SEM images were obtained to further evaluate the morphology and orientation of the crystals obtained.

4.3. Results and Discussion

Polarising microscope: when observed under the crossed Nicols condition, the samples kept showing the same bright and highly oriented pattern as before. It was impossible to make any deduction about the effect of the different temperatures because both sets of samples showed images with the same brightness level.

XRD: XRD patterns of the annealed samples were obtained using the same measuring conditions reported in Paragraph 3.2. Compared to the patterns of the untreated samples (Figure 4.3.1 – 4.3.3), the new ones have the same shape, with three major peaks over a broader peak. In the annealed samples, though, the position of these three peaks was slightly shifted to higher values of 2θ . The higher the temperature of the treatment, the greater the shift. The average shift is limited to 0.24° , leading to an average variation of 0.0020 nm in the distance calculated by Bragg's diffraction law. The thermal treatment also led to a variation in the intensity of the peaks, with a different effect between the samples treated at 150°C and the ones at 200°C : in the samples annealed at 150°C (Figure 4.3.1), a great increase in the intensity of the central peak can be observed, whereas for the other two, if we take into account the difference in baseline, no real difference can be seen. In the patterns of samples annealed at 200°C (Figure 4.3.2), the increase in the intensity of the central peak is greater than what was observed for the samples treated at 150°C . Additionally, the increase in the intensity of the central peak is followed by a light decrease in the intensity of the other two peaks. These results can be interpreted as a greater increase in crystallinity in the samples annealed at 200°C . Since the position of the peaks has not changed significantly from its original value of 2θ , it is possible to assume that the TPCO molecules have the face-on orientation also after the annealing process. Considering that the objective is to fabricate photovoltaic devices, this is an important result. Many researchers ^[24-28] have demonstrated that the face-on orientation of organic conjugated molecules leads to increased efficiency of OPVDs thanks to the overlapping of π -electrons in the vertical direction, which is the direction that separates the two electrodes of the device. As a comparison, thermal treatment of samples without the friction-transferred PT layer was conducted at 200°C (Figure 4.3.3). In this case the intensity of the peaks does not change significantly. This fact is in accordance with the thermal properties of T4P previously shown, where the recrystallisation peak of the DTA analysis is observed around 320°C , while no transformation occurs at 200°C . In addition to the orientation effect on the untreated samples, the PT layer is proved to be responsible, along with the heat, for the enhancement in crystallinity of the TPCO layer. Figure 4.3.4 summarises the effect of the PT layer on the crystallinity of T4P both before and after the thermal treatment at 200°C , which is, for now, the best temperature of the two.

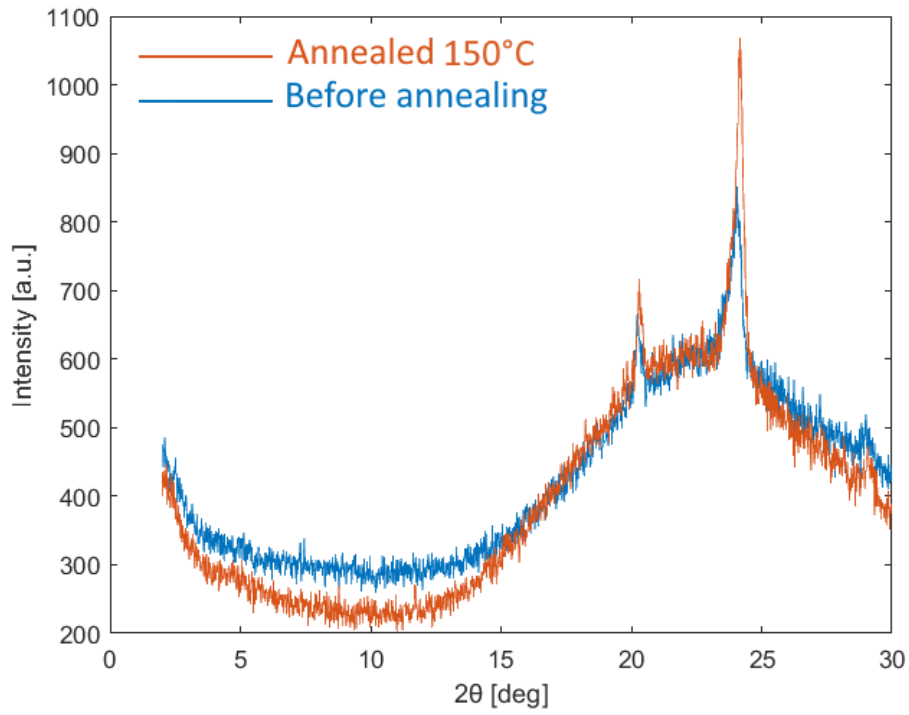


Figure 4.3.1. XRD patterns of the T4P layer deposited on friction-transferred PT before (blue line) and after (red line) annealing at 150°C

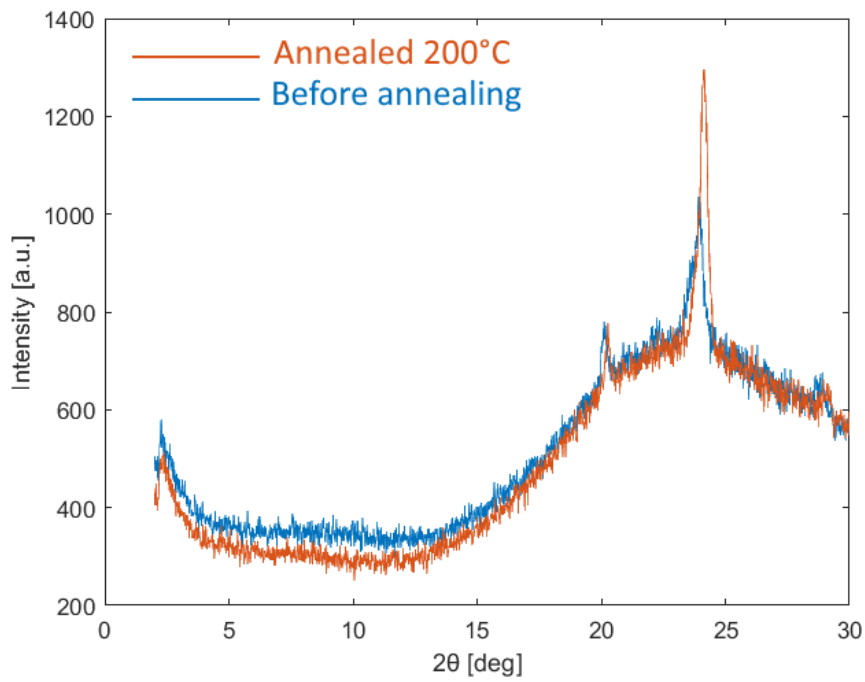


Figure 4.3.2. XRD patterns of the T4P layer deposited on friction-transferred PT before (blue line) and after (red line) annealing at 200°C

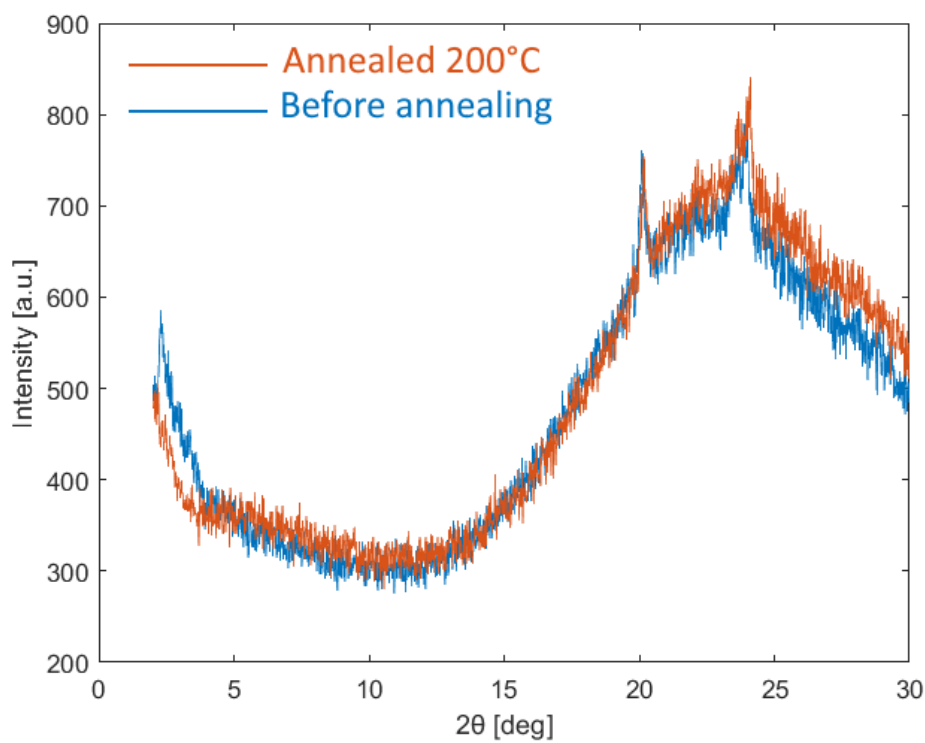


Figure 4.3.3. XRD patterns of the T4P layer (without FT) before (blue line) and after (red line) annealing at 200°C

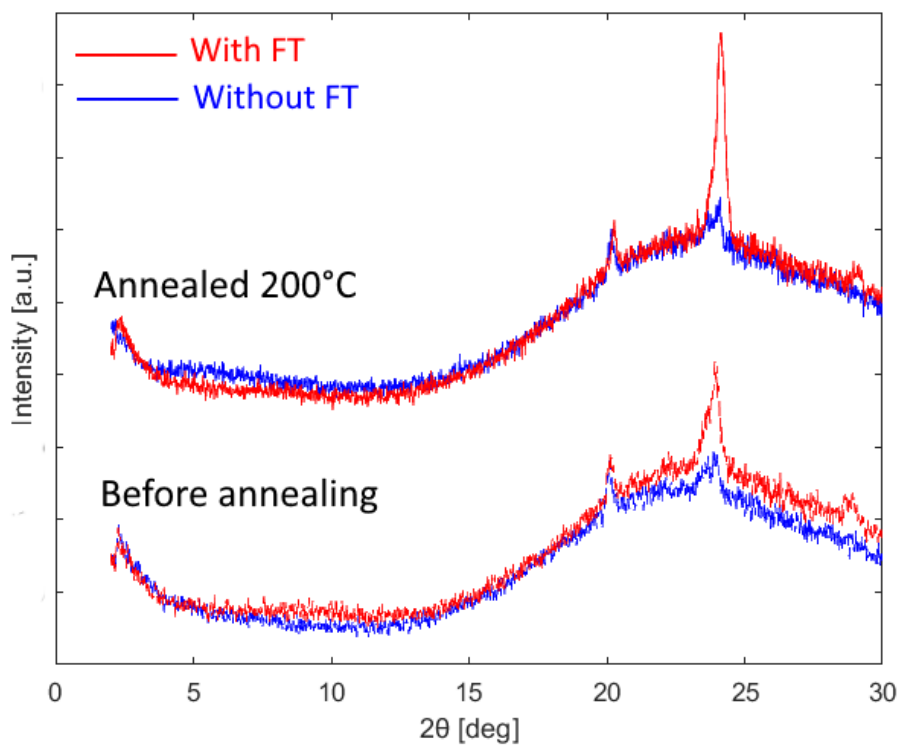


Figure 4.3.4. Comparison of the XRD patterns of the T4P layer deposited on substrates with and without the FT layer, before and after being thermally treated at 200°C

SEM: SEM images of the thermal treated T4P layer were obtained through secondary electron scanning. By the comparison of the top view of the samples annealed at 150 °C and 200 °C (Figure 4.3.5), the XRD data is confirmed: samples annealed at 150 °C, in fact, show a crystal structure that is not as fully developed as the one in the samples annealed at 200 °C. Figure 4.3.6 (a-c), instead, shows the top view of the sample without the FT layer and annealed at 200 °C, while Figure 4.3.6 (d-f) shows the same view for a sample with friction-transferred PT annealed at 200 °C as well. In the former case it is possible to see the presence of a crystalline phase casually dispersed in the organic layer. The crystals are needle shaped, with a dimension of few micrometres, and do not show a favourite orientation. The crystalline phase is surrounded by an amorphous phase. On the other side, the sample with the FT layer shows a microcrystalline structure where crystals are aligned along the FT direction and grow with the longer dimension perpendicular to the FT direction. The crystals are almost 500 nm wide and a few nanometres thick. Even in the material phase between the crystals it is possible to see small nanometric crystallites oriented in the same direction. The cross-section view in Figure 4.3.7 shows the block shape of the crystals and the high roughness of the layer, alternating blocks and valleys (note that the sample was slightly tilted to obtain that picture, so the height of the crystals cannot be evaluated properly). These images, along with the XRD data, confirm the formation of T4P crystals after the thermal treatment. The crystal structure observed is really promising for the creation of photovoltaic devices. The further deposition of an n-type semiconductor will allow to create an interpenetrated structure which is fundamental for enhancing the efficiency of an OPV device ^[9-12]. When the cross section of the samples annealed at 150 °C was observed, instead, only a few crystals were seen, and the TPCO layer was almost uniform, without any block or valley.

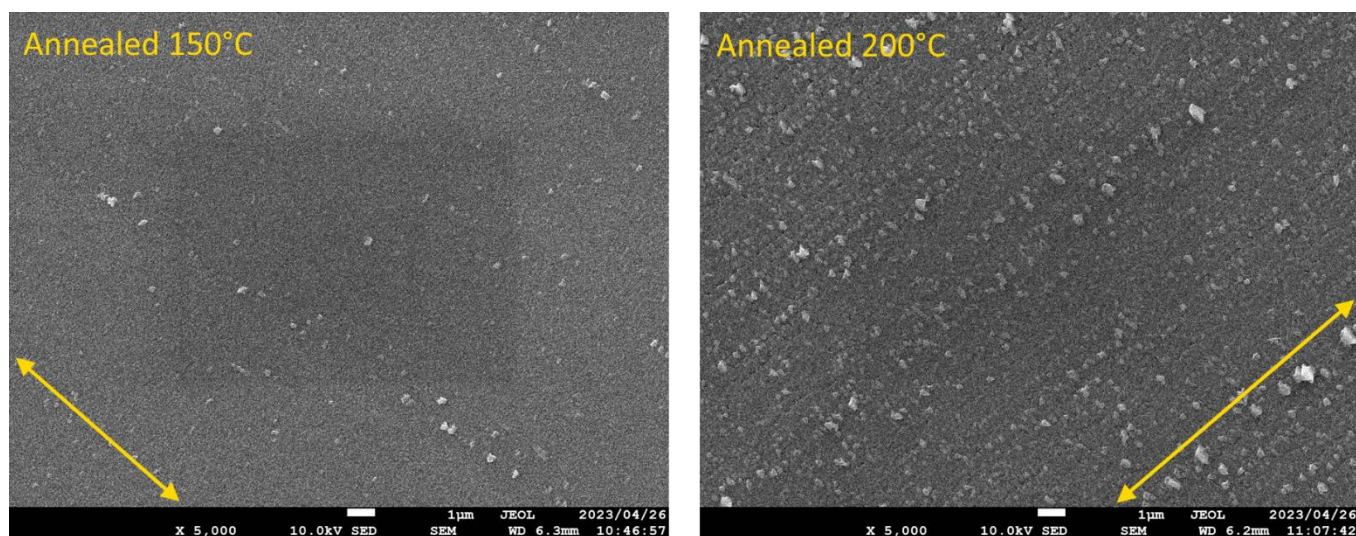


Figure 4.3.5. SEM images of the thermally treated TPCO layer. The yellow arrow indicates the friction transfer direction

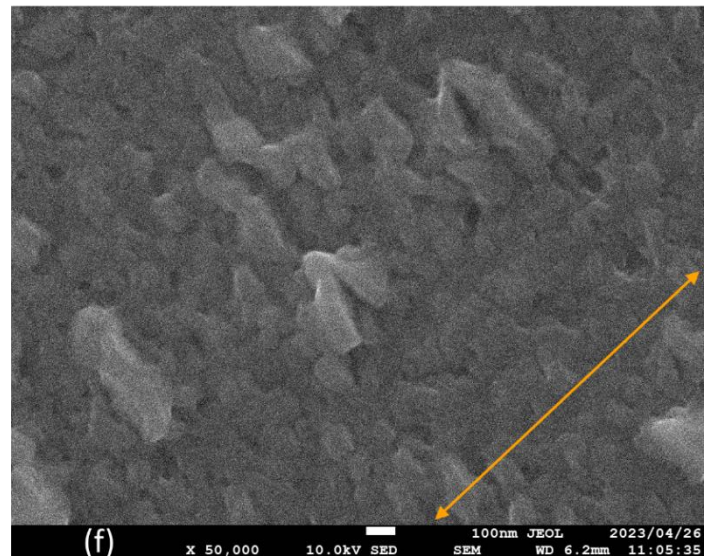
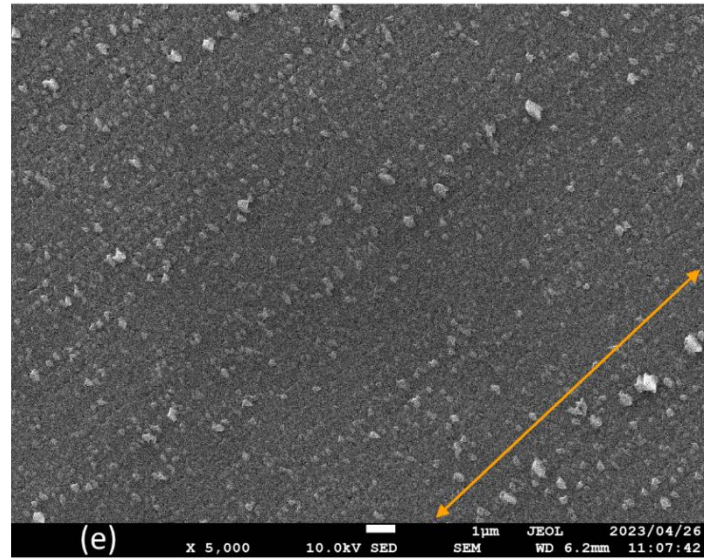
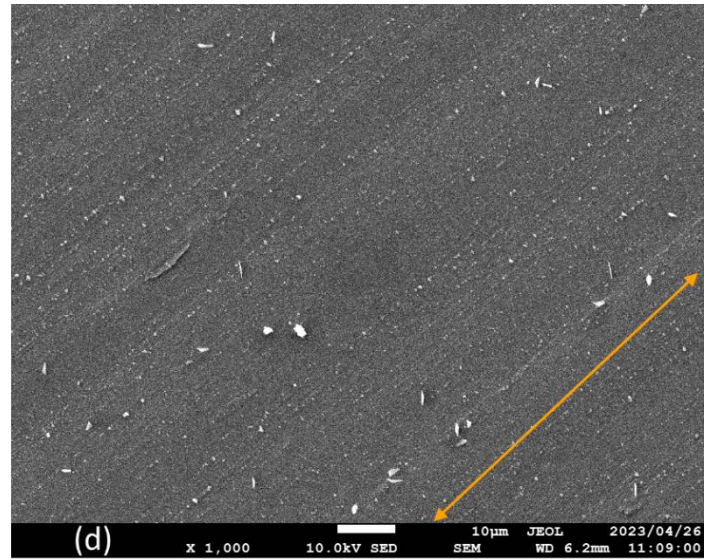
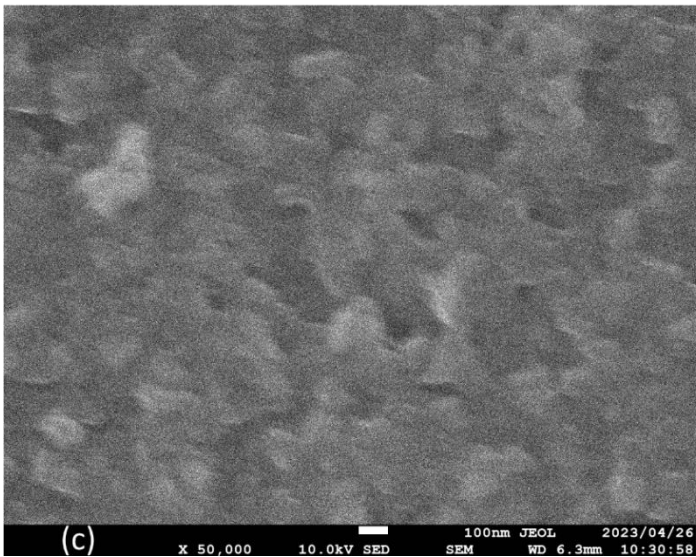
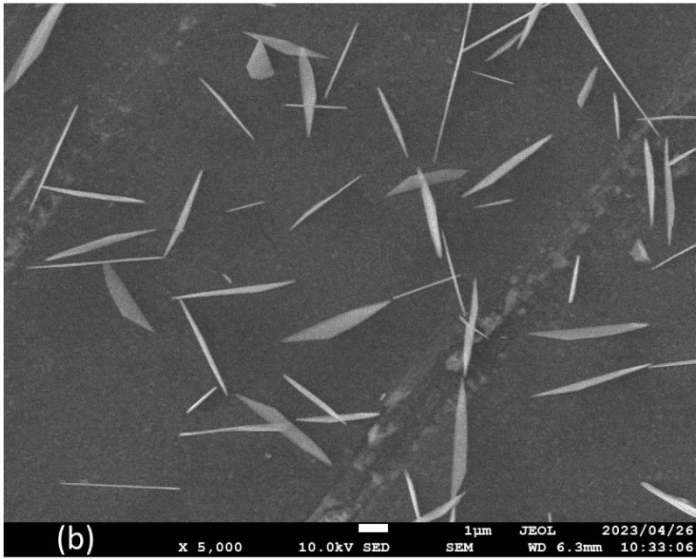
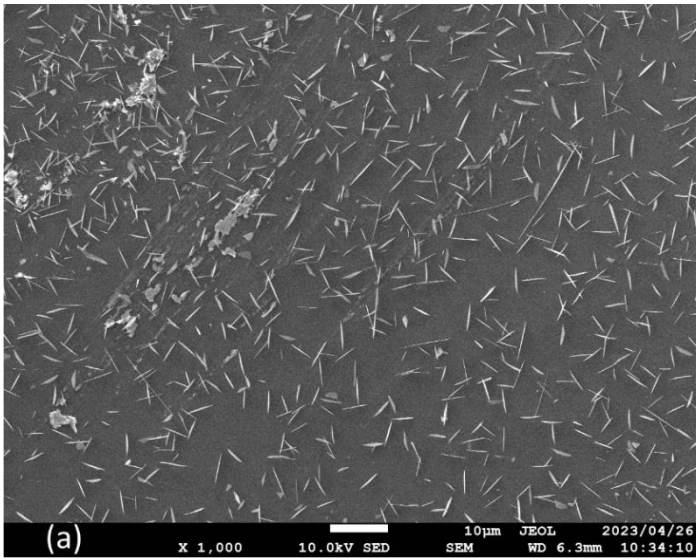


Figure 4.3.6. SEM images of the T4P layer without the friction transfer layer (a,b,c) and deposited on top of friction transferred PT (d,e,f) obtained with different magnifications. The arrow indicates the FT direction

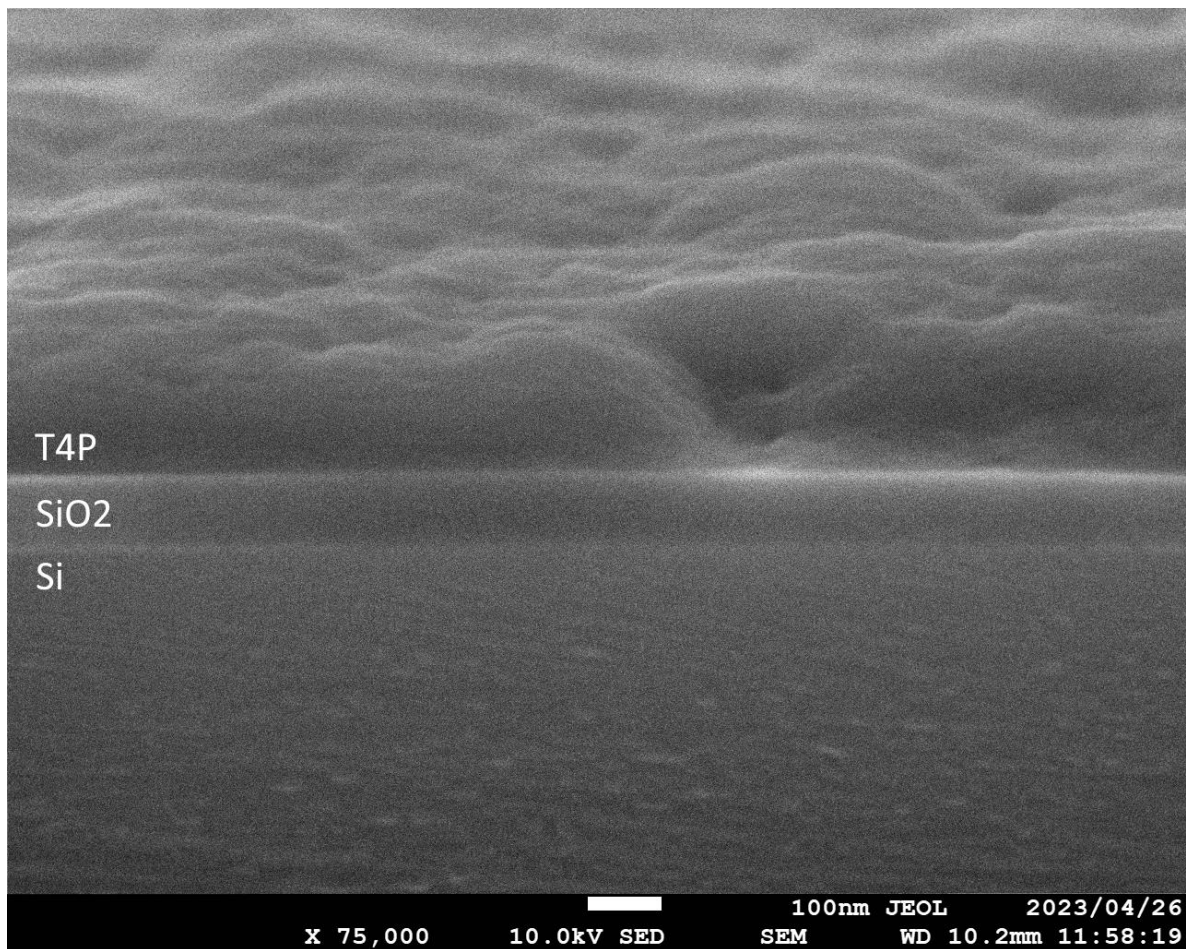


Figure 4.3.7. Cross-section SEM image of the T4P layer deposited on the FT layer. The direction of the FT is coming out of the plane of the picture. Note: the image was taken tilting the sample by 5°.

Polarised absorption spectra: the analyses have been conducted on the annealed samples realised on quartz substrates with the same conditions described in Paragraph 3.2. For the same reasons described previously, the results (Figure 4.3.8 – 4.3.9) show measuring errors that do not allow to calculate the exact DR or F. The samples without the friction transfer layer (Figure 4.3.8) show coincident values of parallel and perpendicular absorbance. When compared to the spectra obtained before the thermal treatment, it is possible to observe a broadening of the absorption peak and an overall increase in the value of absorbance. The formation of non-oriented micrometric crystals can explain this behaviour, as their bigger dimensions lead to an increase in the absorbance. A similar effect is expected in the samples with the FT layer, but the results (Figure 4.3.9 (a,b)) show a significant decrease in absorbance instead. Keeping in mind the possibility of baseline errors that could increase the difference between the pre- and post-treatment absorbance, the cause of this intensity decrease could still be related to the crystallization process: considering the structure seen in the SEM section, when the block-like crystal is originated, the surrounding area has very few material left. The valleys between each block could be deep enough to have just very thin layers of T4P on the substrate. This way, the absorption of those areas is very low, compensating for the increased absorption of the crystals. Regardless of the decrease in absorbance, though, the annealed samples still show dichroism. The higher the annealing temperature, the higher the values of DR. It is also possible to notice that, when the temperature is increased, the absorption band of T4P becomes wider. This

effect is caused, again, by the crystallisation process: inside the crystals, T4P molecules are strongly aligned with a face-on orientation. This orientation is parallel to the dipole moment of the molecule, so the absorbance is also increased at higher wavelengths. Considering that the treatment at 200 °C brings a higher level of crystallinity, it is then normal that the samples annealed at 200 °C (Figure 4.3.9 (b)) not only have greater absorption, but also show a broader peak, with an absorbance spectrum that adds up to the PT one.

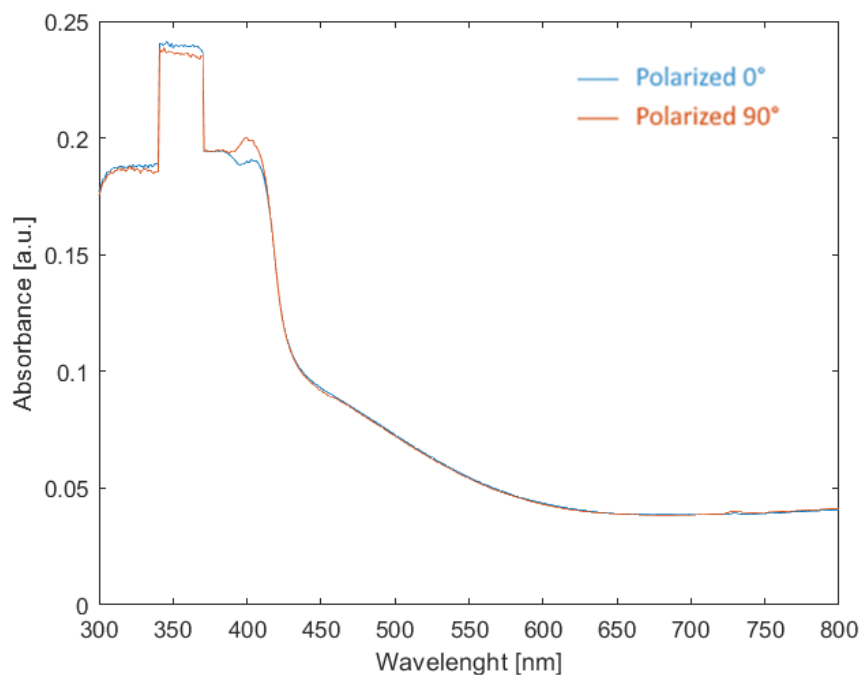


Figure 4.3.8. Polarised absorption spectra of T4P, deposited on a clean quartz substrate (without FT), and annealed at 200 °C

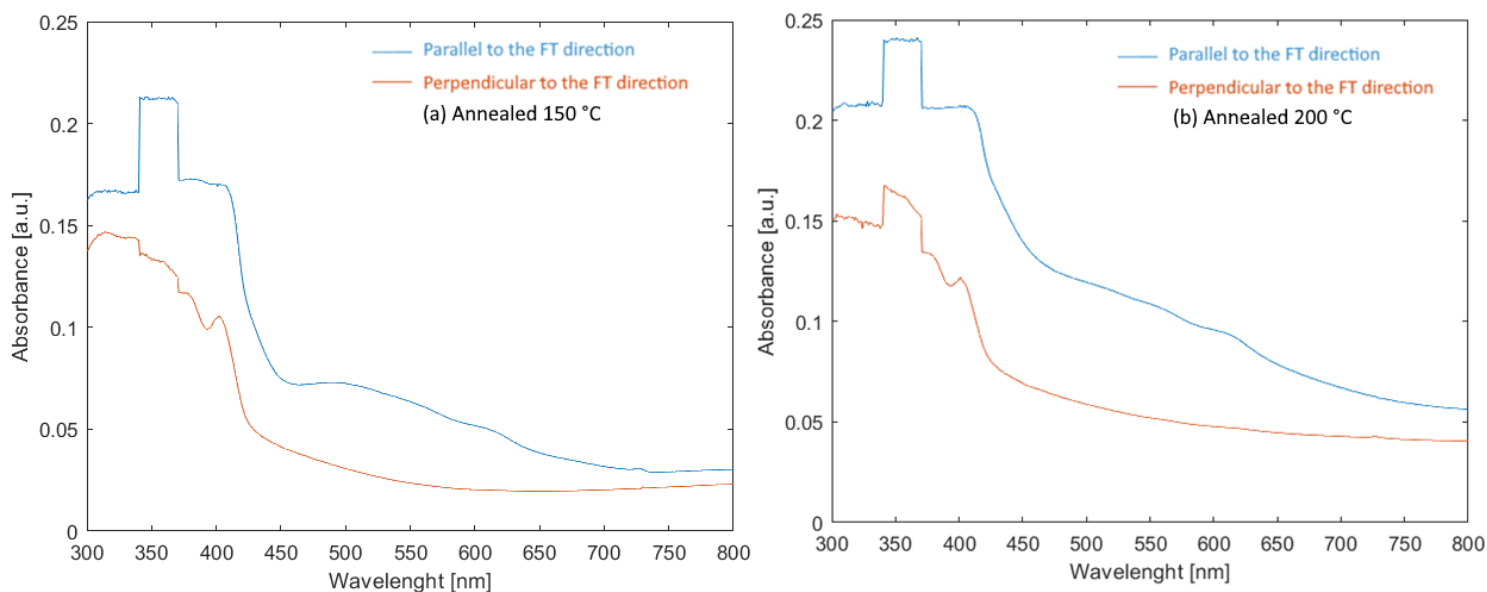


Figure 4.3.9. Polarised absorption spectra of T4P, deposited on friction-transferred PT, annealed at (a) 150°C and (b) 200°C

Chapter 5 – Production of OPV devices

5.1 Device structure

The device configuration is illustrated in Figure 5.1.1 (a). The entire structure was created on top of a 15x15 mm glass/ITO patterned substrate. The ITO pattern, shown in Figure 5.1.1 (b), was 150 nm thick and constitutes the bottom electrode of the device. The fabrication of the device started by depositing the thin PT orientation film by friction transfer, followed by T4P (the p-semiconductor) and by fullerene C₇₀ (the n-semiconductor). Bathocuproine (BCP) was deposited between the semiconductor and the top electrode. Being a transparent, wide-gap electron transporter, BCP acts as an exciton blocking layer, preventing the cathode quenching. The entire structure is then closed by the top Al electrode. As shown in figure 5.1.1 (c), the final device was a square of 4 mm² area, and four devices were created on each substrate.

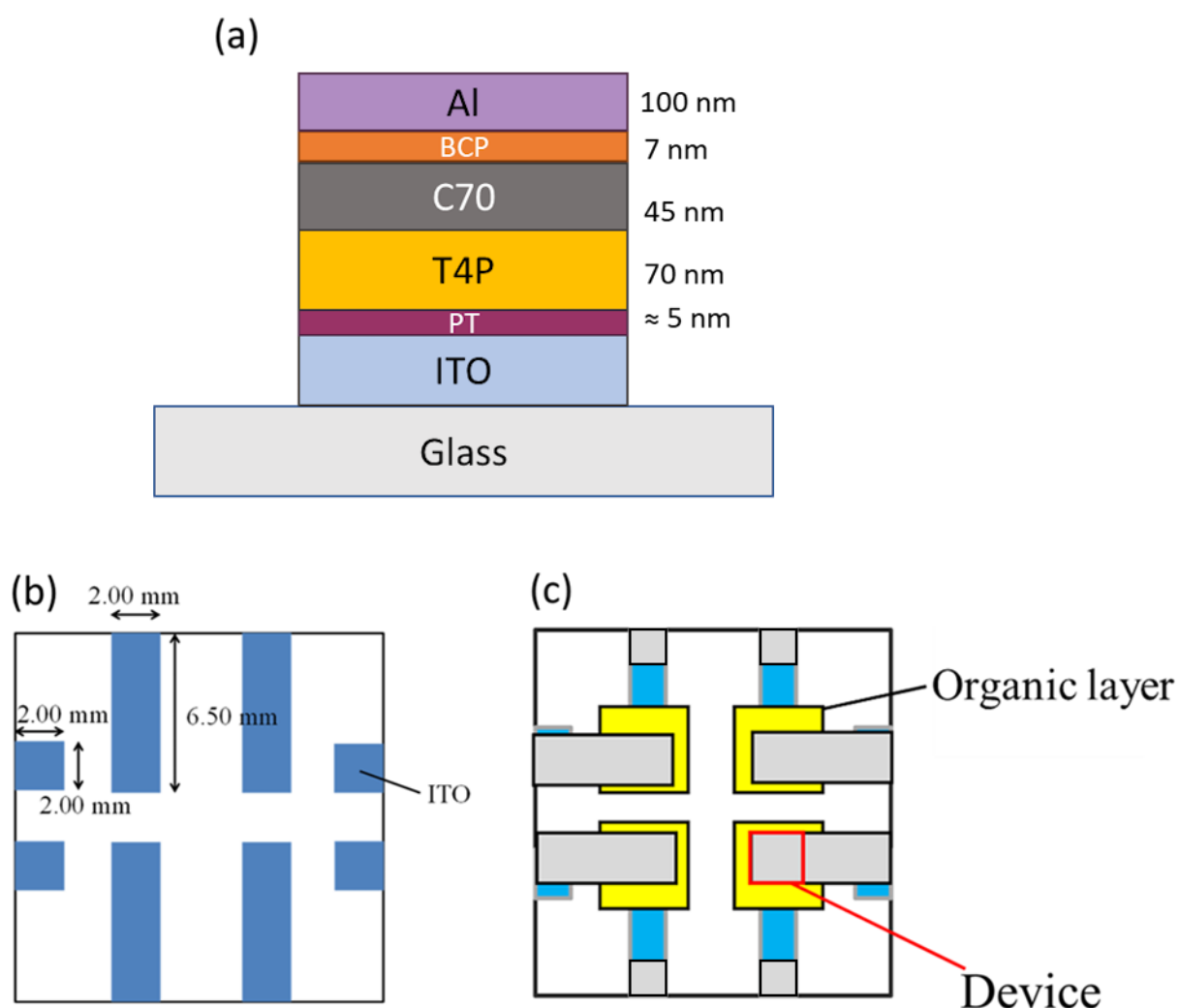


Figure 5.1.1. (a) Schematic illustration of the device structure. (b) Geometry of the ITO pattern on the glass substrate. (c) Top view of the substrate after the deposition process. Four devices were obtained on each substrate

5.2 Experimental

Before depositing PT by the friction transfer method, the glass/ITO substrates were cleaned by sonicating for 5 minutes in different organic solvents (in order: acetone, isopropanol, ethanol) and in distilled water, repeating each step twice. Nitrogen gas was blown to dry the substrates and, finally, UV-Ozone cleaning was performed for 10 minutes.

The friction transfer of PT was carried out using the same method discussed in Chapter 2 and the result was again a very thin and highly oriented film (Figure 5.2.2). The presence of a small step between glass and ITO pattern causes the material to accumulate on the side of the electrode, but, being outside of the actual device area, it is not going to cause any problem.

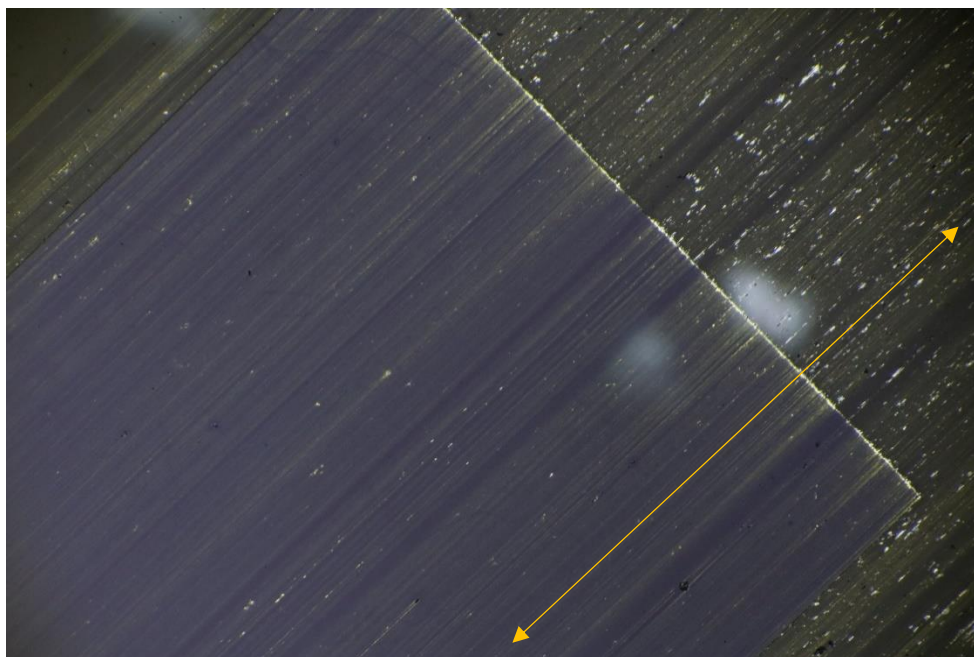


Figure 5.2.2. Polarizing microscope image at 5x magnification of the friction-transferred PT layer over the glass/ITO substrate. The arrow indicates the direction of the friction transfer

The deposition of the organic layers was performed under vacuum at pressures in the order of 10^{-4} Pa, using a metallic mask with four squared holes (yellow area in Figure 5.1.1 (c)), and with a deposition rate between 0.01 – 0.03 nm/s. The first to be deposited was T4P, with a thickness of 70 nm. Usually, OPVDs have a much thinner semiconductor layer, but, in this case, the thermal treatment causes a great change in the profile shape of the TPCO layer with the peaks getting taller and the valleys getting deeper. This migration of organic material might generate valley areas without T4P at all if the TPCO layer was too thin. Since we wanted to make sure a p-n junction is present all over the surface of the device, this higher thickness was chosen. After the deposition of T4P, the samples were moved into a glovebox with a nitrogen atmosphere without exposing them to air. Inside the glovebox the mask was removed and the samples were annealed for 1 hour at 200 °C, while keeping the oxygen level of the box below 50 ppm and a dew point of less than -30 °C. Once the process was finished, the samples were brought inside the vacuum chamber again with the same metallic mask. C₇₀ and BCP were subsequently deposited, with a final thickness of 45 and 7 nm respectively. The samples were moved again inside the glovebox where the mask was changed and brought back inside the deposition chamber for the final deposition of 100 nm of aluminium. Once this last step was completed, the devices were moved again into the glovebox, where they were kept under a nitrogen atmosphere with an oxygen level of less than 500 ppm and a dew point lower than -20 °C.

Six glass/ITO substrates were used, so 24 devices were fabricated simultaneously. To evaluate the effect of the friction transfer and of the thermal treatment on the electronic properties, these devices were fabricated in different ways, as explained in Table 5.2.1.

Substrate	Device Number	Friction Transfer	Thermal Treatment
d01	1-4	-	-
d02	5-8	○	-
d03	9-12	○	-
d04	13-16	-	○
d05	17-20	○	○
d06	21-24	○	○

Table 5.2.1. Processing conditions of the fabricated devices

Electrical measurements of the devices were performed in the glovebox under the same conditions described above. To confirm the presence of a p-n junction, a voltage between -0.5 – 1.5 V was applied to the aluminium electrodes in the dark. The photovoltaic properties were evaluated, instead, exposing the bottom part of the device (glass/ITO side) to simulated sunlight AM 1.5 G (intensity of incident light equal to 100 mW/cm²). The analyses were also performed with polarised light by putting a polariser between the samples and the light source.

5.3 Results and Discussion

Results of the electric measurements are illustrated in Figures 5.3.1 – 5.3.4, and the main characteristics of each type of OPVD are summarised in Table 5.3.1. Starting from the devices created on substrate d01 (no FT and no thermal treatment), we can see in Figure 5.3.1 that all four devices work as photodiodes and are capable of generating electrical power. The average value of short circuit current J_{sc} was -0.5 mA/cm^2 , while the open circuit voltage was 0.46 V . The average power conversion efficiency (PCE) was 0.12% , with a fill factor (FF) of 0.2618 . These values are lower than the ones Taniguchi et al. [29] found in their work. The device structure is almost the same, the only difference between the two is the thickness of the T4P layer, which, in their case, was 15 nm . This is the reason why the value of V_{oc} is almost the same, but the PCE is much lower: as explained in Chapter 1, when creating a planar heterojunction, a thicker semiconductor layer is less efficient than a thinner one. Therefore, having a T4P layer almost five times thicker than what they reported can easily explain why the present devices have a PCE that is one order of magnitude smaller than the one they reported. The presence of the polarised causes a significant attenuation of the incident light, giving a

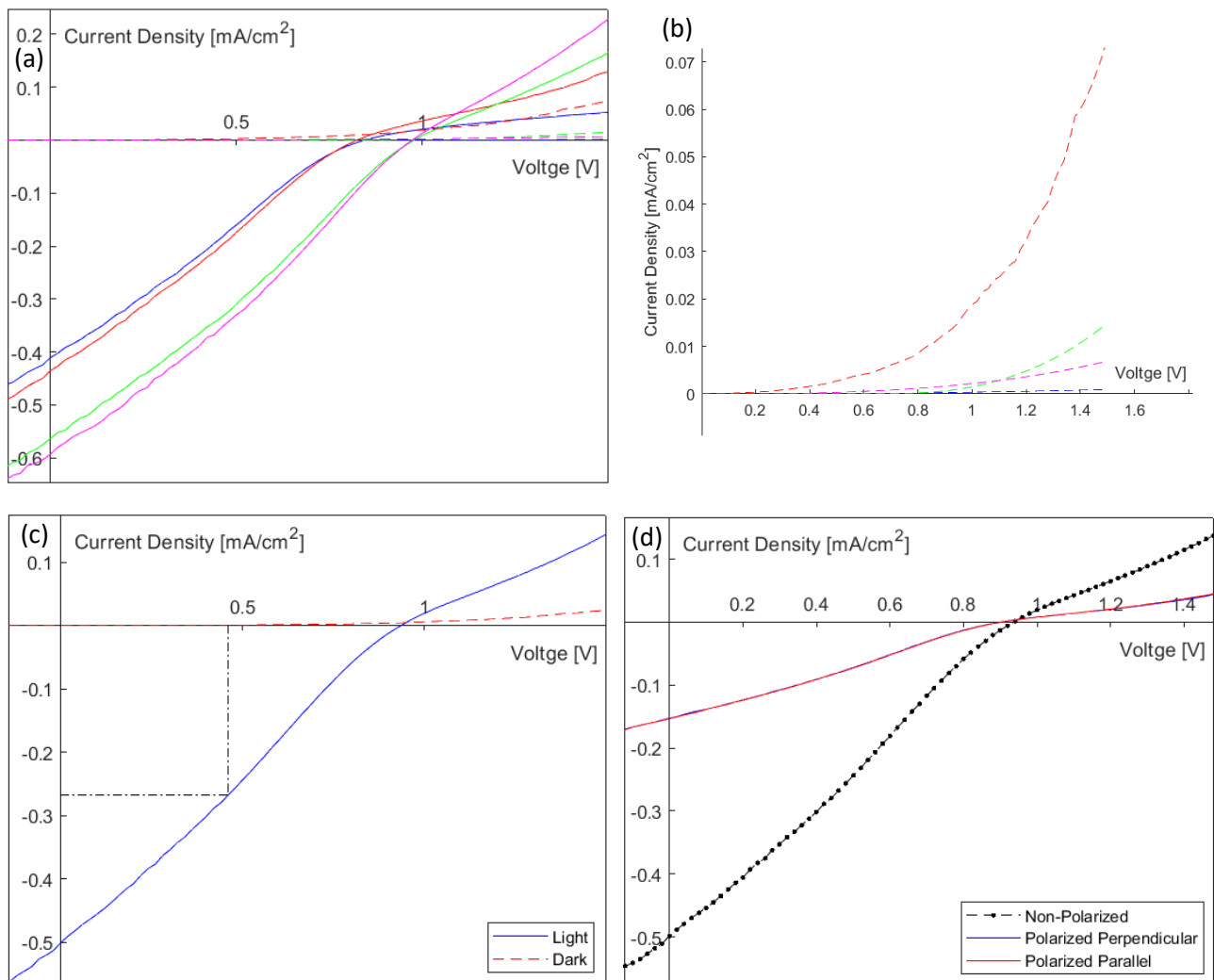


Figure 5.3.1. J-V characteristics of devices 1 – 4 **(a)** under light (continuous line) and in the dark (dashed line), **(b)** in the dark. **(c)** Average J-V characteristic of the four devices under light (continuous line) and in the dark (dashed line), with indications of the maximum current density and voltage used for calculating the PCE.

(d) Average J-V characteristic under polarised and non-polarised light

lower photocurrent generation, but, since there is no prevalent orientation, it is completely normal that the polarisation direction does not influence the J - V characteristic.

The results obtained for the devices 5-8 (d02 – with FT and no thermal treatment) are the first ones to get far from what was expected. As shown in Figure 5.3.2, the devices work as photovoltaic devices, but their performances are much lower than those found for devices 1–4. These devices had an average $J_{sc} = -0.243 \text{ mA/cm}^2$, $V_{oc} = 0.5 \text{ V}$, and $\text{PCE} = 0.02\%$. Measurements of the devices fabricated on substrate d03 led to similar results. The main issues are two: the presence of an orientation template should increase the PCE due to a higher molecular orientation of the semiconductor, even if there is no thermal treatment to enhance the crystallinity^[19,24]. Secondly, if the semiconductor is actually oriented, then there should be a difference between the two polarised characteristics, but, in the present case, however, there is none.

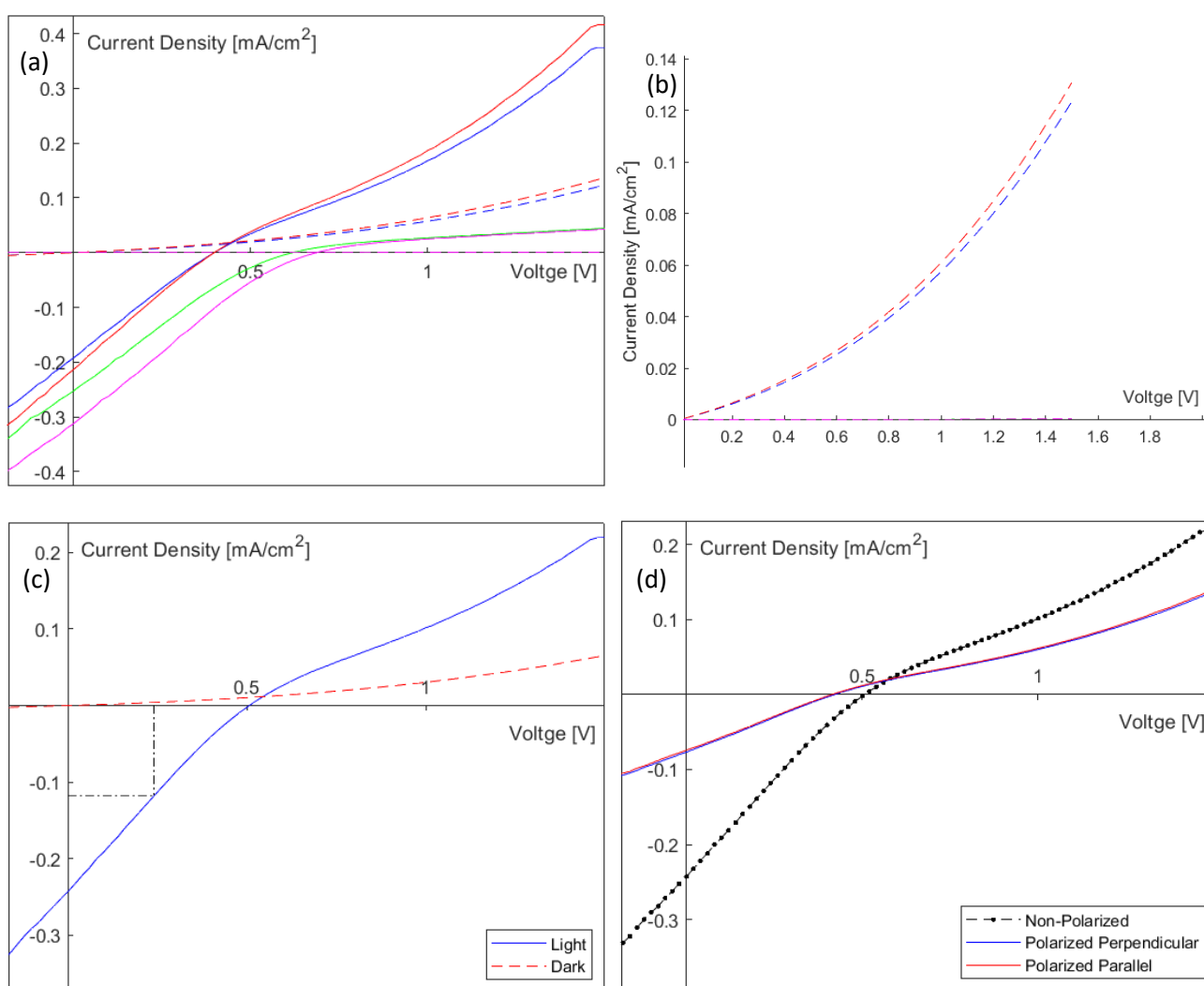


Figure 5.3.2. J - V characteristics of devices 5 – 8 **(a)** under light (continuous line) and in the dark (dashed line), **(b)** in the dark. **(c)** Average J - V characteristic of the four devices under light (continuous line) and in the dark (dashed line), with indications of the maximum current density and voltage used for calculating the PCE. **(d)** Average J - V characteristic under polarised and non-polarised light

Figure 5.3.3 illustrates the J - V characteristics of the devices fabricated on substrate d04 (13-16 – Without FT, with thermal treatment). These devices show even lower performances than the previous ones, having an average PCE of 0.009% and a very strange J - V characteristic. Having no clues about what happens during the thermal treatment of this specific structure, it is for now impossible to draw any conclusions about this type of behaviour.

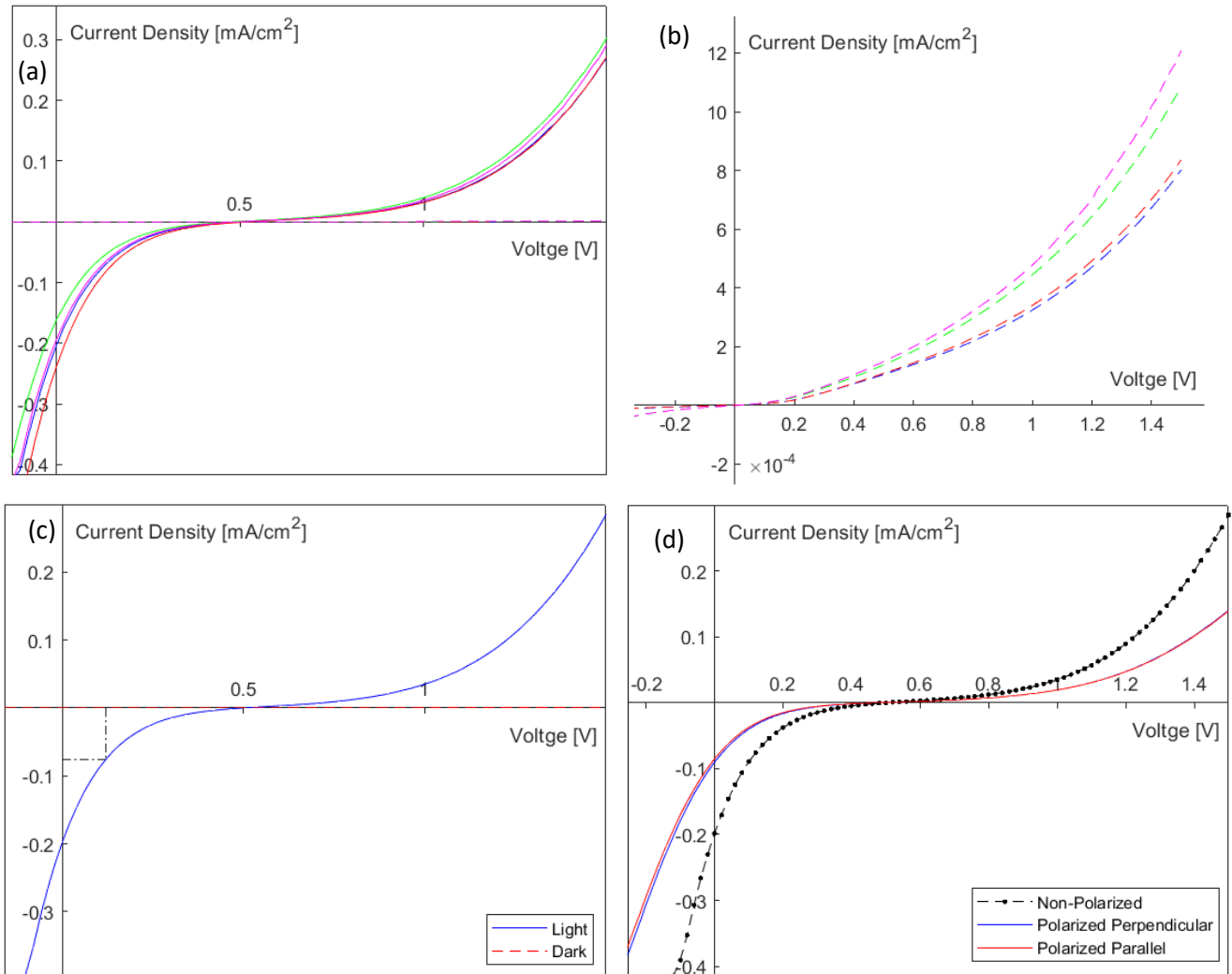


Figure 5.3.3. J - V characteristics of devices 13 - 16 **(a)** under light (continuous line) and in the dark (dashed line), **(b)** in the dark (note that the vertical axis is multiplied by 10^{-4}). **(c)** Average J - V characteristic of the four devices under light (continuous line) and in the dark (dashed line), with indications of the maximum current density and voltage used for calculating the PCE. **(d)** Average J - V characteristic under polarised and non-polarised light

Lastly, the electrical measurements performed on the devices fabricated on substrate d05 and d06 (17- 24 – With FT and thermal treatment) resulted in two different types of J - V characteristics, both illustrated in Figure 5.3.4. In one case, the devices showed a typical diode behaviour, both in the dark and under the light, with no power generation; in the other case, the devices showed the characteristic of an almost zero-resistance resistor, with a current flow that was entirely dependent on the measuring instrument's compliance (maximum current limitation). The former case (Figure 5.3.4. (a)) shows a different behaviour in the dark and under the simulated sunlight, therefore it is reasonable to believe that there is photocurrent generation at the p-n junction, but the device does

not generate any power. On the other hand, in the case of Figure 5.3.4 (b), a short circuit of the device should be the case of such behaviour.

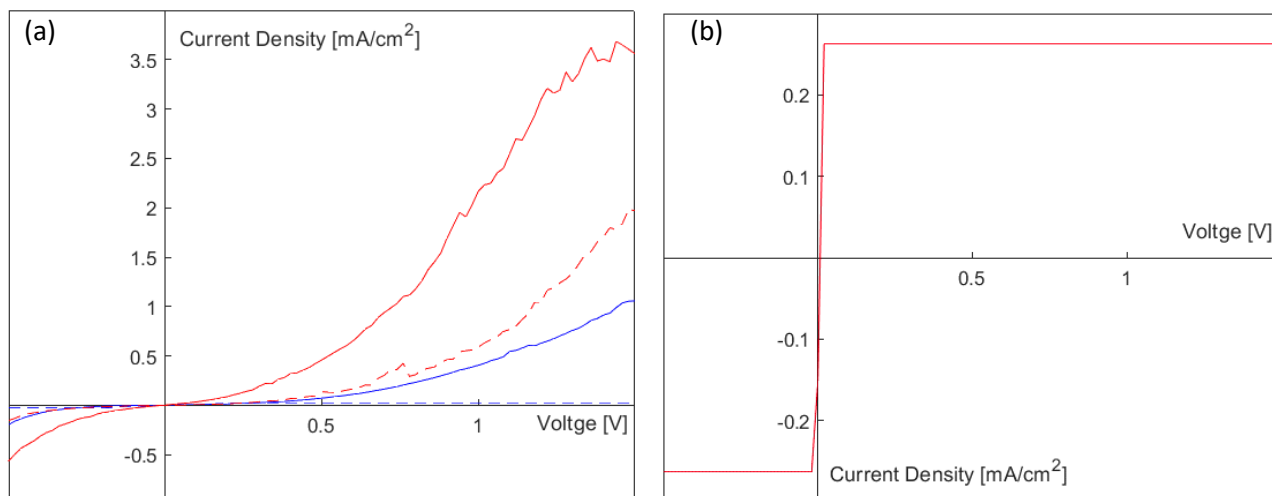


Figure 5.3.4. Different types of J-V characteristics obtained by devices 17-24 (with FT and thermal treatment). In (a) the characteristics obtained in the dark are represented with a dashed line

Substrate	V_{oc} [V]	V_{max} [V]	J_{sc} [mA/cm ²]	J_{max} [mA/cm ²]	PCE [%]	FF
d01	0.94	0.46	- 0.5	- 0.268	0.12	0.2618
d02	0.5	0.24	- 0.243	- 0.118	0.028	0.2335
d03	0.62	0.26	- 0.229	- 0.109	0.028	0.1994
d04	0.5	0.12	- 0.198	- 0.076	0.0091	0.0921
d05	-	-	-	-	-	-
d06	-	-	-	-	-	-

Table 5.3.1. Main photovoltaic properties of the fabricated devices

To explain the results shown above, different hypotheses have been made: first of all, to explain why the presence of the FT layer lowers the efficiency of the devices, we have to look at the energy levels of HOMO and LUMO of the different materials composing the solar cell. The energy diagram is shown in Figure 5.3.5. Here, it is possible to see that PT's HOMO is almost aligned with ITO's energy level. This means that, in normal conditions, there is almost no potential barrier and very easy charge transport between the two. It has been reported that the UV-O₃ treatment is actually modifying the work function of ITO: the longer the treatment, the higher the energetic level (in absolute values) [30,31]. So the overall effect of the ozone cleaning process was to bring ITO's work function closer to T4P's HOMO. This way, not only the charge transport of devices d02 and d03 was lowered, but the performances of devices d01 were actually increased, creating even a bigger difference between the two types of devices. In order to maintain a low energy barrier between ITO and PT, the UV-O₃ treatment should be as short as possible, or avoided at all. There is still an energy gap between PT's HOMO and T4P's HOMO, but it is reasonable to believe that, thanks to the high degree of orientation, PT can act as a hole collection layer, thus maintaining a high level of charge transfer at the interface [25].

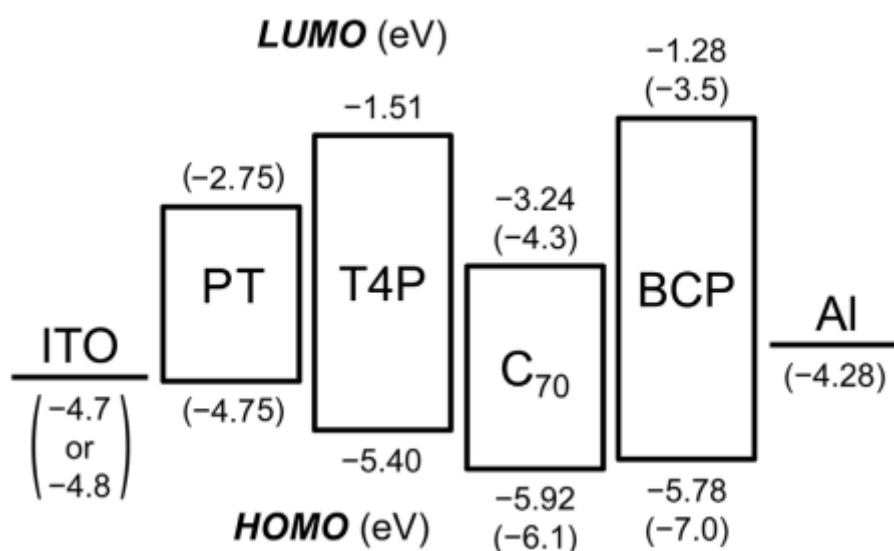


Figure 5.3.5. Energy diagram of the materials used for creating the OPVD. The values between brackets are the energies obtained from literature, while the others were previously calculated by this laboratory

The results showed no difference when using light polarised parallel or perpendicular to the FT direction. To explain this issue, the hypothesis is that the PT orientation template is mostly effective only on the T4P layer, while C₇₀ gets deposited with an almost random orientation. Being the main light absorber, if C₇₀ is not oriented, then most of the power generated will not depend on the polarizing direction. To better understand the degree of orientation, the devices were observed with a polarising microscope (in the air, outside the glovebox) under the crossed-Nicols condition. The images, shown in Figure 5.3.6 – 5.3.8 prove this hypothesis, as it is possible to notice that the friction transfer pattern can be barely seen in the devices on substrate d02 (with FT - Figure 5.3.7), and the non-polarised image is much similar to the one of the devices on substrate d01 (without FT – Figure 5.3.6). The low degree of orientation of C₇₀ on substrate d02 was further confirmed when devices on substrates d05 and d06 (with FT and thermal treatment – Figure 5.3.8) were observed. In this case the friction transfer pattern can be seen clearly even without the crossed-Nicols condition, and appears to be inducing its orientation up to the Al layer. In the literature, a polarisation-dependant absorbance was found for OPVDs based on the FT method, which led to a very different *J-V* characteristic based on the light polarisation^[25]. In such cases, though, the semiconductor layer was much thinner. It is proven that the FT method is much more effective when the material deposited on top of it has a low thickness, so it is impossible to have a direct comparison, or expect similar behaviour.

Lastly, we tried to understand why the devices d05 and d06 (with FT and thermal treatment) were not working as expected. As explained at the beginning of Paragraph 5.2, we chose the thickness of the T4P layer in order to make sure that a T4P layer always remained between C₇₀ and PT after the thermal treatment. Since there is no previous data about the thickness change of T4P during the annealing process, our main hypothesis is that 70 nm is not enough to prevent the formation of those areas without TPCO, or, in most cases, the thickness of T4P in the valley areas is very thin (few nm). This way, when there is direct contact between C₇₀ and PT, the electrical measurements result in a short circuit and a zero-resistance resistor behaviour, whereas, if a small layer of T4P is interposed between the two, the behaviour resembles the one of a diode. To better understand the effect of the thermal treatment on the devices, SEM images of their cross-section were taken. Figure 5.3.9 and 5.3.10 show the cross-section of devices d04 and d01 respectively (note that in the case of substrate

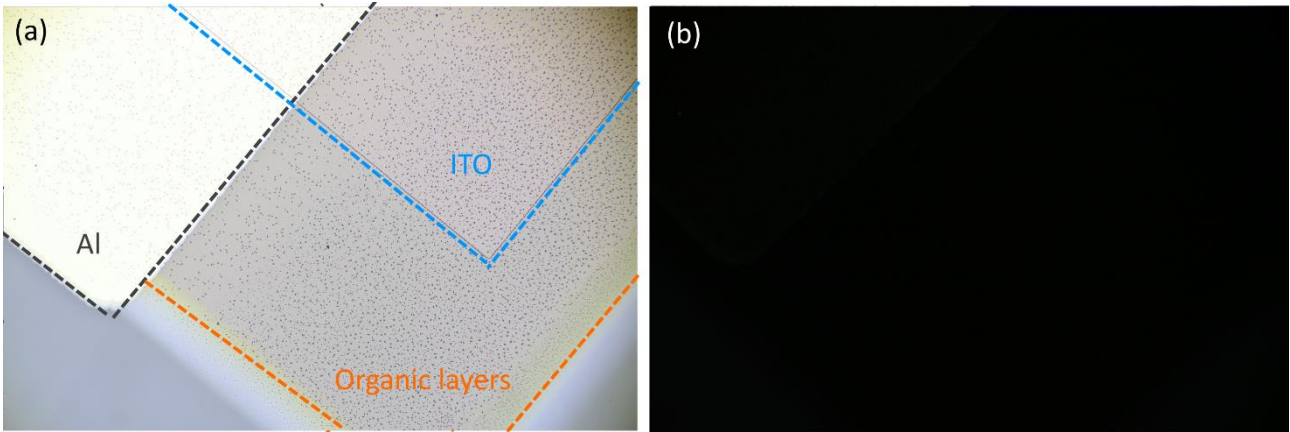


Figure 5.3.6. Polarizing microscope images at 5x magnification of one of the devices fabricated on substrate d01 (no FT, no thermal treatment) under (a) normal conditions and (b) crossed-Nicols

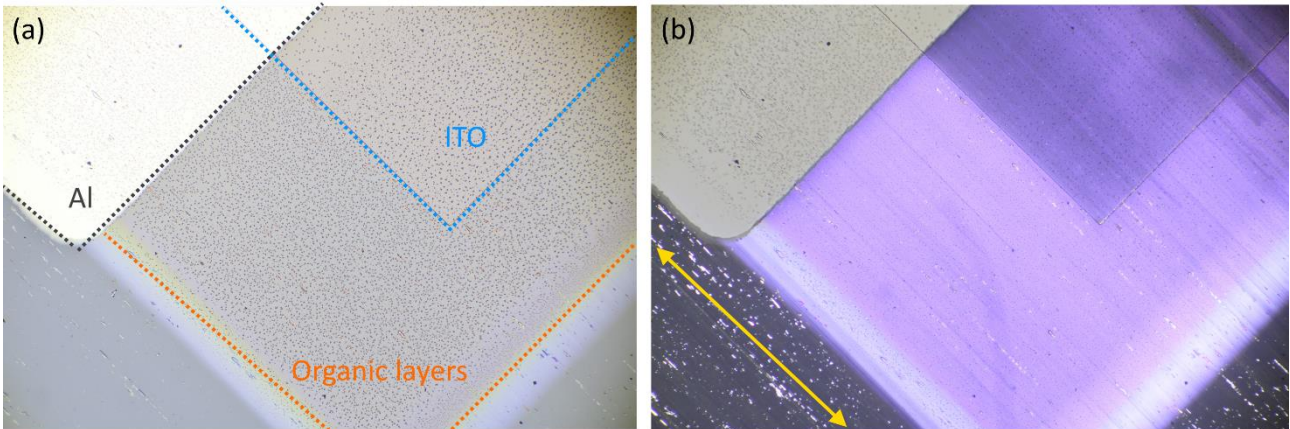


Figure 5.3.7. Polarizing microscope images at 5x magnification of one of the devices fabricated on substrate d02 (with FT, no thermal treatment) under (a) normal conditions and (b) crossed-Nicols. The yellow arrow indicates the FT direction

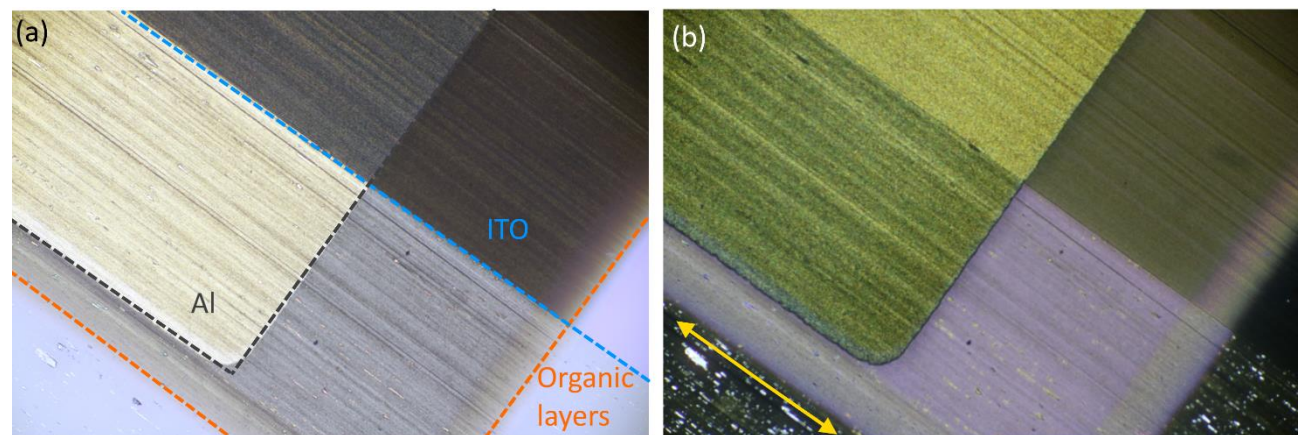


Figure 5.3.8. Polarizing microscope images at 5x magnification of one of the devices fabricated on substrate d04 (with FT and thermal treatment) under (a) normal conditions and (b) crossed-Nicols. The yellow arrow indicates the FT direction

d04 the cross section was taken outside of the actual device area, so there is no Al on top – see the yellow area in Figure 5.1.1. (c)). In the former case, it is immediately possible to recognise the block-like crystal structure originated by the thermal treatment. In this case, the blocks are composed of a bottom layer of crystalline T4P and a top layer of C₇₀ and BCP. The image was taken with a tilt angle of 5°, so no direct measurements can be made, but it is clear that the areas between each crystal have just a very thin layer of material. Considering the possibility that during the deposition the crystals could be blocking the vapour path to these areas, this thin layer must contain around 35-40 nm of C₇₀ and a few nanometers of BCP. If we subtract these from the total thickness of the in-between areas, then the result is that almost no T4P is found there, confirming our previous hypothesis. In the case of devices d01, the presence of a planar heterojunction was confirmed. In both cases, due to the resolution limit of the EDS instrument, it was not possible to perform an elemental analysis and clearly see the junction interface.

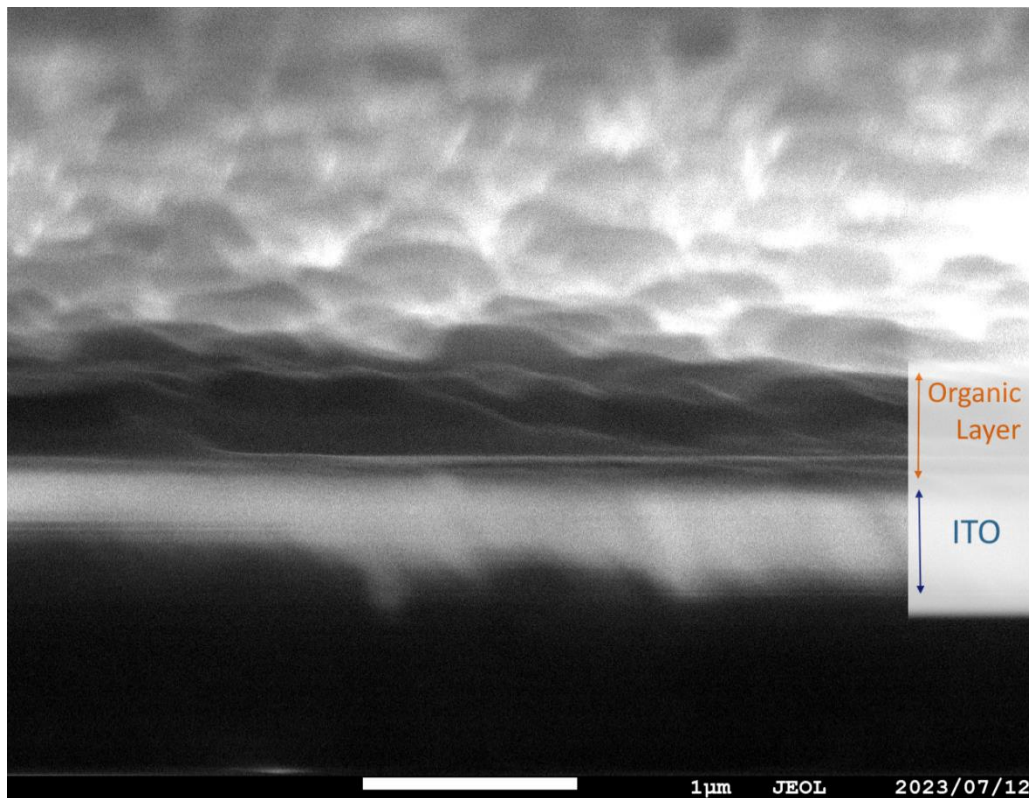


Figure 5.3.9. Cross section SEM image of one of the devices fabricated on substrate d04 (with FT and thermal treatment). The friction transfer direction is perpendicular to the plane of the image. Note that the image was taken outside of the actual device area and with a tilt angle of 5°

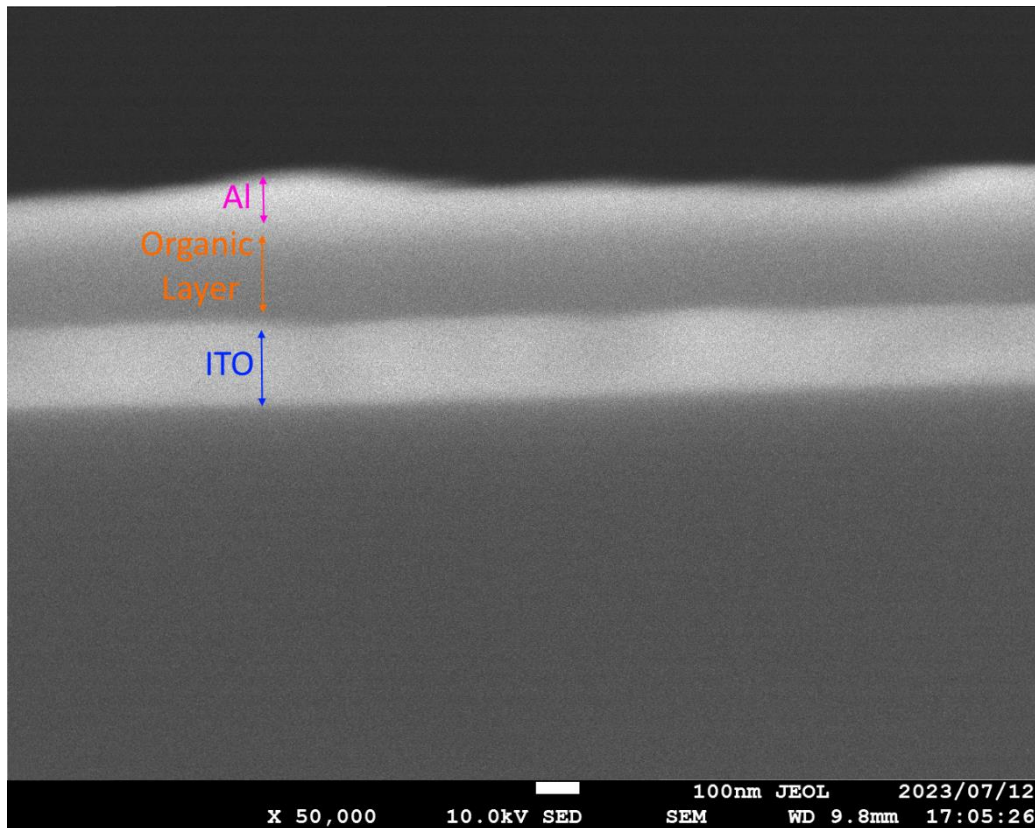


Figure 5.3.10. Cross-section SEM image of one of the devices fabricated on substrate d01 (no FT and no thermal treatment)

5.4 New experimental phase

In light of the results obtained, the fabrication process was modified, and new devices were fabricated. The experimental procedure is the same as the one described in Paragraph 5.2. This time, however, no UV-O₃ treatment was performed, and the deposition of T4P was divided into two steps: 50 nm were first deposited on the devices with and without FT, then the annealing was carried out, and then 20 more nm were deposited. By doing so, we expect that the amorphous T4P deposited during the second step could fill any potential gap between the crystals generated during the annealing. For the samples without thermal treatment, instead, this two-step deposition will bring no changes. Table 5.4.1 contains a summary of the devices created. This way we aim to remove the chances of short-circuiting the annealed devices.

Substrate	Device Number	Friction Transfer	Thermal Treatment
Nd01	25 – 28	-	-
Nd02	29 – 32	○	-
Nd03	33 – 36	-	○
Nd04	37 – 40	-	○
Nd05	41 - 44	○	○

Table 5.4.1. Processing conditions of the new devices fabricated

5.5 New Results and Discussion

Results of the electric measurements are illustrated in Figures 5.5.1 – 5.5.5, and the main characteristics of each type of OPVD are summarised in Table 5.5.1.

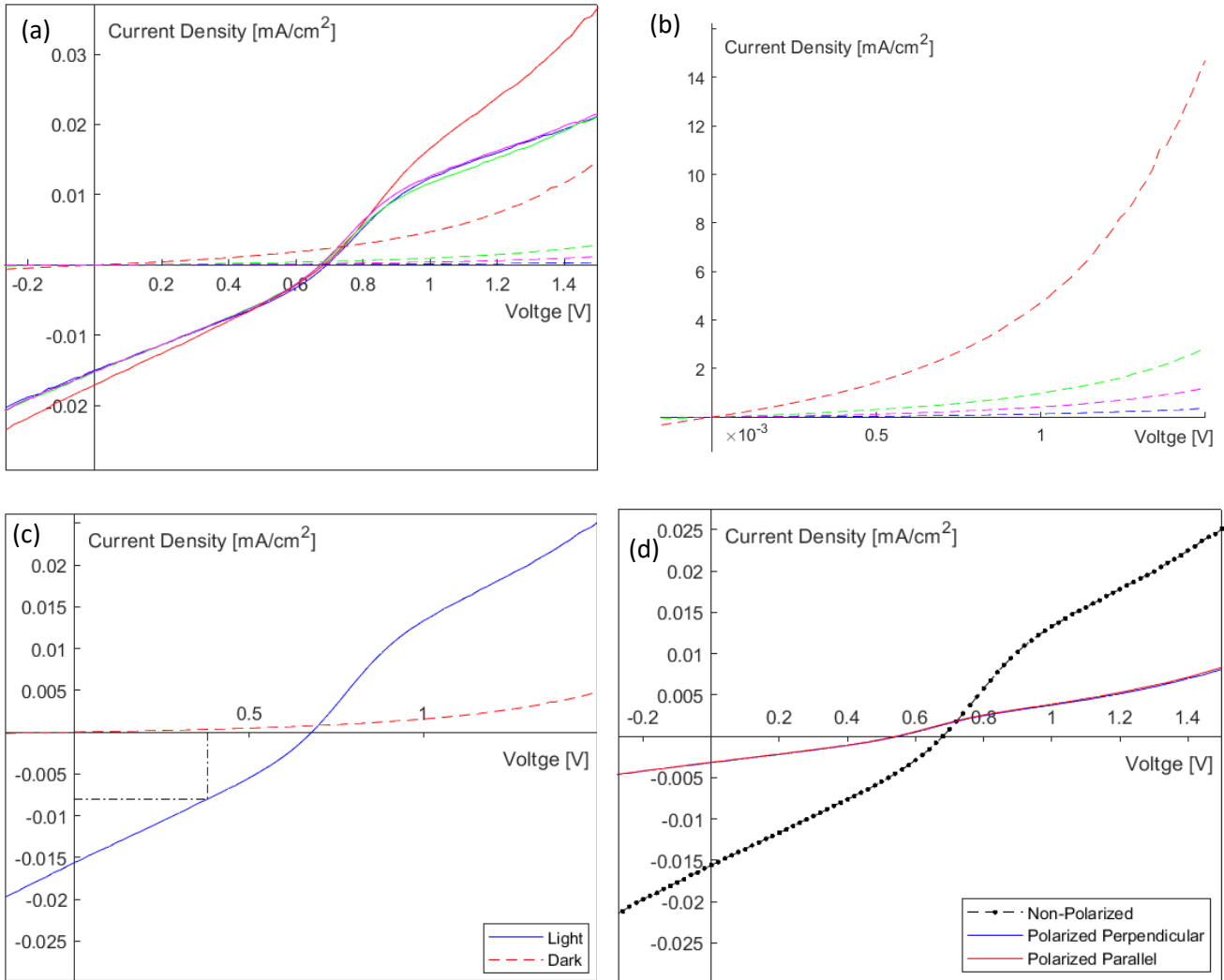


Figure 5.5.1. *J-V characteristics of devices 25 - 28 (a) under light (continuous line) and in the dark (dashed line), (b) in the dark. (c) Average J-V characteristic of the four devices under light (continuous line) and in the dark (dashed line), with indications of the maximum current density and voltage used for calculating the PCE. (d) Average J-V characteristic under polarised and non-polarised light*

Figure 5.5.1 (a-d) shows the *J-V* characteristics of devices 25 – 28 (no FT and no thermal treatment). Compared to devices d01, we can see a light increase in the V_{oc} but a significant decrease in J_{sc} , getting one order of magnitude lower. Such low values of current flow led to an average value of PCE of 0.003 %. First, we attributed this huge decrease to a large energy potential barrier between ITO and T4P caused by the lack of UV-O₃ treatment. The results obtained from the other devices, though, tell us that this is not the case, since all the OPVDs created with the new experimental method show values of current density that are one order of magnitude lower than those obtained from the previous devices. The last thing to point out about device Nd01 is that, as expected by the lack of the friction transfer layer, there is no different response to light polarisation.

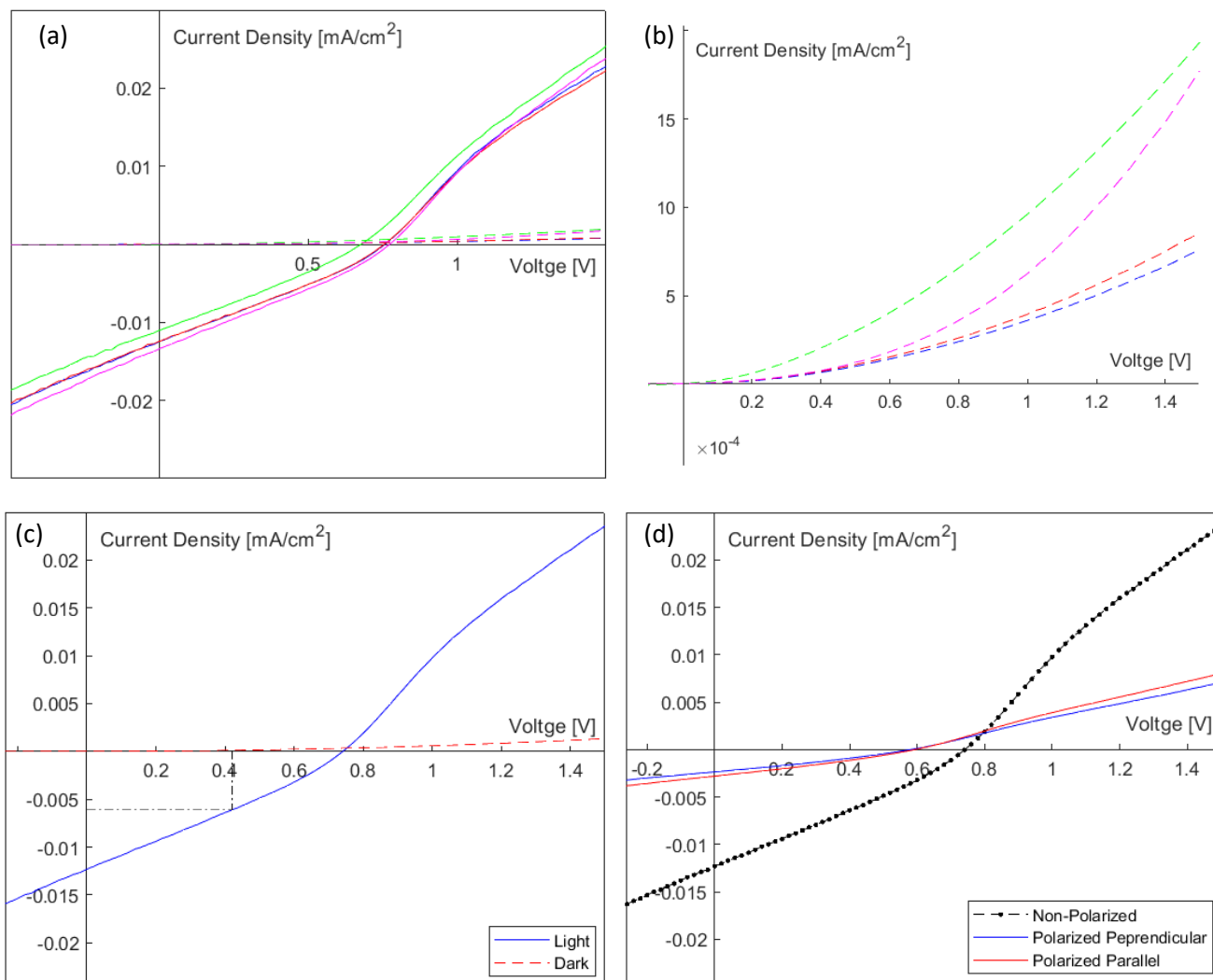


Figure 5.5.2. *J-V characteristics of devices 29 - 32 (a) under light (continuous line) and in the dark (dashed line), (b) in the dark. (c) Average J-V characteristic of the four devices under light (continuous line) and in the dark (dashed line), with indications of the maximum current density and voltage used for calculating the PCE. (d) Average J-V characteristic under polarised and non-polarised light*

The devices Nd02 (with FT and no thermal treatment) showed electrical characteristics similar to the devices Nd01 described above. As illustrated in Figure 5.5.2 (a-d), the values of J_{sc} are slightly lower, but the higher values of V_{oc} are compensating, so the overall PCE is similar. Compared to the previous devices (d02), instead, while J_{sc} is more than ten times lower, V_{oc} has increased from 0.5 V to 0.74 V. While there may be many possibilities behind the former decrease, the increase in open circuit voltage might be associated to a better alignment of the energy levels of ITO and PT. The most noticeable property of these devices is that the polarised analyses show different behaviour when the light is polarised parallel or perpendicular to the friction transfer direction. The difference is not big, but the device is showing better properties when light is polarised parallel to the FT direction.

Devices 33 – 36 (without FT, with thermal treatment) are the first ones to have a *J-V* characteristic much different from the previous devices. While devices d03 had such an unusual curve profile, devices Nd03 (Figure 5.5.3) have an electrical characteristic resembling the one of normal photovoltaic devices. If, on the one hand, the new experimental method fixed this aspect, on the

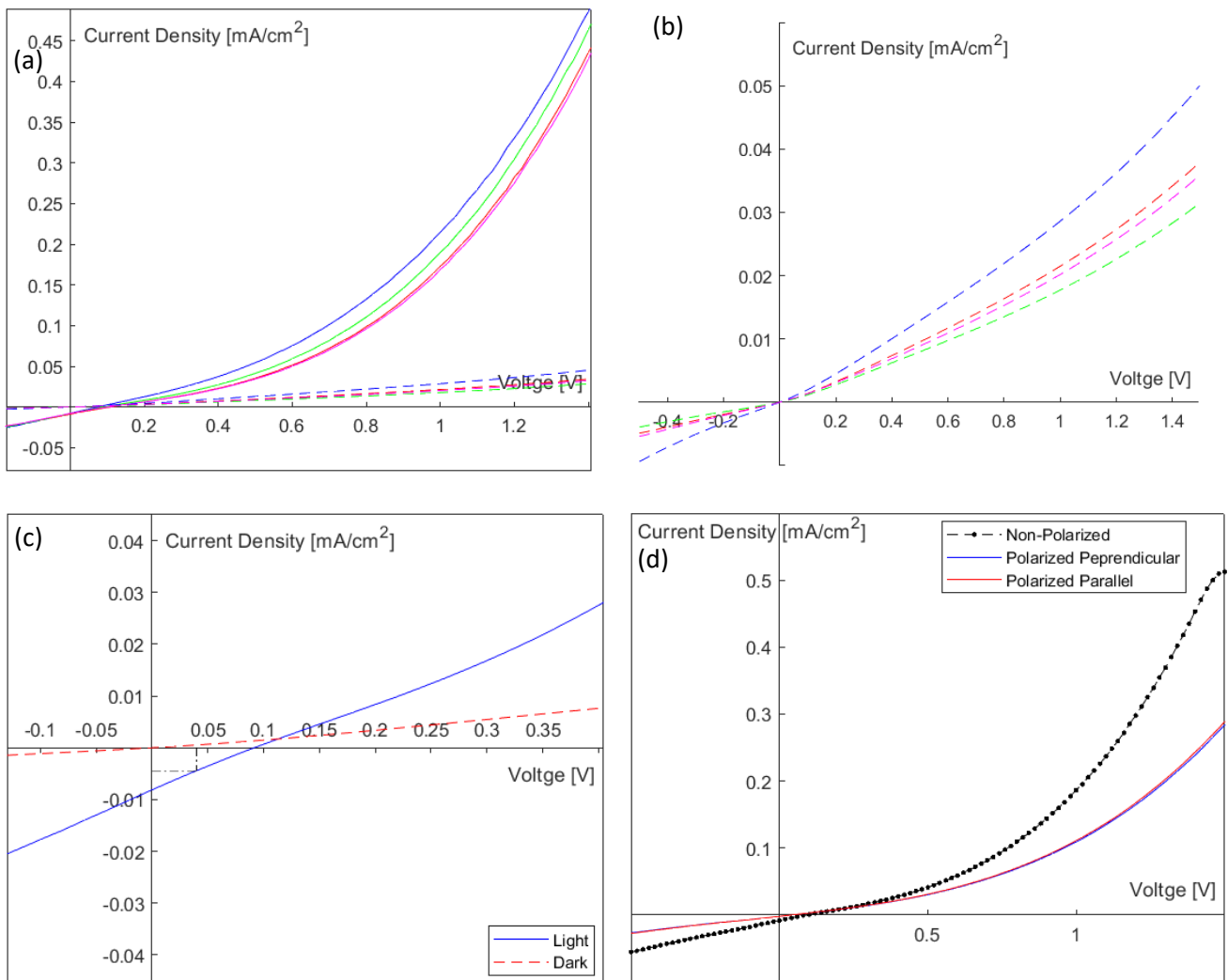


Figure 5.5.3. J-V characteristics of devices 33 - 36 **(a)** under light (continuous line) and in the dark (dashed line), **(b)** in the dark. **(c)** Zoom in of the average J-V characteristic of the four devices under light (continuous line) and in the dark (dashed line), with indications of the maximum current density and voltage used for calculating the PCE. **(d)** Average J-V characteristic under polarised and non-polarised light

other hand, though, the results are still not the expected ones: having values of $J_{sc} = 8.1 \cdot 10^{-3}$ mA/cm² and $V_{oc} = 0.1$ V, the devices have a PCE of $1.75 \cdot 10^{-4}\%$. Power generation is minimal, even though there is still a big difference between the results under the light and in the dark. As expected, polarised analyses show the same results, indicating no preferential orientation. It is worth noting that, even if lacking power generation, the current density values manage to reach the same order of magnitude as the previous devices.

Devices 37 – 44 (Nd04 and Nd05 – with FT and thermal treatment) have almost identical properties. Figure 5.5.4 shows the results obtained from the devices on substrate Nd05. Since no device showed short circuit characteristics, we can say that the new experimental procedure successfully solved that problematic. On the other hand, however, we obtained devices with zero PCE and a photodiode behaviour again. As for the d05 and d06 cases, the current density is highly influenced by the presence of light, but even though they reach the highest values of current density among the new devices, the overall values of J in devices Nd04 and Nd05 are much lower than the ones of d05 and d06. Moreover, no dependence on the polarisation direction was found.

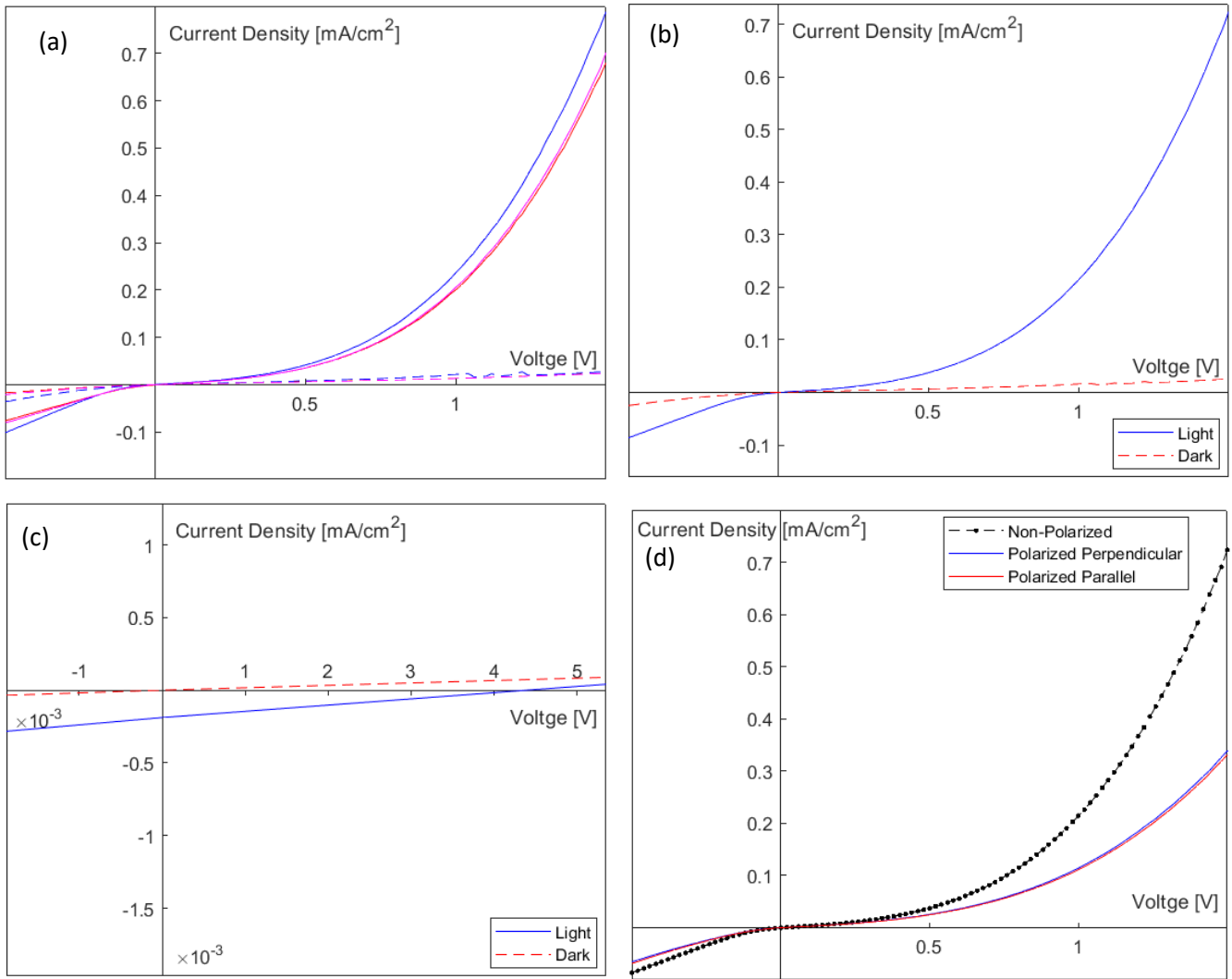


Figure 5.5.4. J-V characteristics of devices 41 - 44 **(a)** under light (continuous line) and in the dark (dashed line). **(b)** Average J-V characteristic of the four devices under light (continuous line) and in the dark (dashed line). **(c)** Zoom in of the average J-V characteristic. **(d)** Average J-V characteristic under polarised and non-polarised light

Substrate	V_{oc} [V]	V_{max} [V]	J_{sc} [mA/cm ²]	J_{max} [mA/cm ²]	PCE [%]	FF
Nd01	0.68	0.38	- 0.0156	- 0.0080	0.00305	0.2877
Nd02	0.74	0.42	- 0.0123	- 0.0061	0.00257	0.2828
Nd03	0.1	0.04	- 0.0081	- 0.0044	$1.75 \cdot 10^{-4}$	0.2164
Nd04	-	-	-	-	-	-
Nd05	-	-	-	-	-	-

Table 5.5.1. Main photovoltaic properties of the newly fabricated devices

While, on the one hand, the new experimental method allowed us to solve some issues, such as the presence of short circuits, on the other hand, it has downgraded the performances of the devices. The main causes can be found in the misalignment between the energy levels of ITO-PT-T4P and in the quality of the heterojunction created. In the first case, though, there are examples in literature with a similar situation: Mizokuro et al. ^[19] have created OPVDs based on ITO / PEDOT:PSS / friction-transferred PT / α -6T. Their research reports a HOMO level of 5.3 eV for 6T, which is close to the 5.4 eV of T4P, while PEDOT:PSS has a HOMO level around 5.1 eV. The overall device structure is much different, because it is based on thinner layers and no thermal treatment, but from the energy levels point of view, the situation is much similar to the one presented in this research. We assume that misalignment between the energetic levels of ITO-PT-T4P has a minimal impact, even though it is clear that removing the UV-O₃ treatment did not improve the device properties. It is probable that the presence of impurities on the electrode's surface has a much more negative influence on the device properties than the energetic levels mismatch, so, in the future, the UV-O₃ cleaning should be performed at least for a short amount of time.

Instead, SEM analyses of the cross-sections of the devices were performed again for a better understanding of the heterojunction quality. Since we noticed that the thermal treatment of the T4P film was always causing a great reduction in PCE of the device and brought closer to a diode behaviour, this time we focused on devices Nd03 and Nd05. The two structures are similar, but a more significant aggregation of T4P was induced in device Nd03 where the absence of the FT layer caused the formation of more irregular crystals. In both cases we saw the presence of organic materials between the crystals. As for the previous SEM analyses, the resolution limit of the EDS instrument was not enough to allow us to distinguish between the different materials, but, based on the thickness, we can assume that the two-steps deposition of T4P was effective, as confirmed also by the lack of short circuits in the devices. However, by observing both the images and the associated *J-V* characteristics, our main hypothesis is that even though T4P creates a block-like crystal structure, the C₇₀ layer is not creating an interpenetrated heterojunction, but it is just following the surface profile of T4P. In addition, the thickness of the organic layer is much higher than it should be. The theoretical thickness of the organic layer should be around 126 nm (with a few nanometres of error due to the irregularity of the FT layer), but the cross-section images show a thickness that is almost twice as much. So, even though the rough crystalline surface increases the interfacial area between the two semiconductors, the increased thickness is drastically lowering the conversion efficiency. The thicker semiconductor layer is instead enhancing light absorption. When light gets absorbed by the device, excitons are generated inside the organic layer. These particles are neutrally charged but can be dissociated into an electron-hole pair if they reach the interface. As explained in Chapter 1, an increased thickness of the active layer reduces the probability of charge separation. When the dissociation takes place, the applied potential separates the free charges, which then move to the electrodes. However, since neither power generation nor light emission are present, we assume that this structure promotes charge recombination at the interface. We hypothesise that during the time between the exciton dissociation and the hole-electron recombination, the charge density inside the semiconductors is much higher than usual, so the whole conductivity of the material is improved. The current flow, though, is composed only by the intrinsic carrier of the material, while the free charges generated by the photovoltaic effect decay rapidly due to the recombination process. Under these terms, we can think about the light absorption as a doping mechanism of the semiconductor. This way, it is possible to explain why the devices work as photodiodes, having a behaviour that is more suitable for a photodetector application rather than a photovoltaic device.

Conclusions and future perspectives

Thin films of oriented organic material were created by the friction transfer method. Not only was the friction-transferred layer demonstrated to be highly anisotropic, but it was also proved to induce the same orientation on the materials deposited on top of it. This peculiar characteristic was used to obtain highly oriented films of T4P by simply vapour-depositing the TPCO molecules on top of an FT layer of PT. As confirmed by XRD, SEM and polarized absorption analyses, thermal treatment at 200 °C was found to induce crystallization of T4P and thus to further increase the degree of molecular orientation. The final structure consisted of microcrystalline arrays, oriented along the friction transfer direction and with a block-like shape that looks ideal for creating an interpenetrated bulk heterojunction. Organic photovoltaic devices based on this structure were created. The device architecture consisted of ITO/PT/T4P/C₇₀/BCP/Al. As a comparison, devices without friction transfer and/or without thermal treatment were created as well. The results showed that the devices with a simple planar heterojunction had a higher PCE than the ones with FT or with FT and thermal treatment. This last type of devices, in particular, mainly showed malfunctioning due to the presence of short circuits. In order to obtain working and more efficient devices, the experimental procedure was changed, and new devices were fabricated. Even though the new OPVDs were working, their performances were much lower than the ones of the previous devices. Moreover, even if functional, devices with FT and thermal treatment did not work as photovoltaic devices. Their J-V characteristics, instead, resembled the one of a photodetector, having a diode behaviour where the current density had a strong dependency on the presence of incident light.

We still believe that TPCOs and the friction transfer method can make a difference and be used for creating highly efficient photovoltaic devices. In order to be able to clearly understand why the final devices were not generating any electrical power, studies about the crystallization progress of T4P need to be carried out. Knowing the correlation between the annealing parameters and the change in thickness and size of the crystal can be extremely helpful in defining the device architecture. The thermal treatment could also be improved, trying to see if temperatures between 200 and 250 °C can bring to even higher molecular orientation. Finally, the experimental procedure for the device creation could be changed again: depositing the n-semiconductor by spin coating could be the solution for obtaining the interpenetrated bulk heterojunction that we were looking for, and, consequently, to obtain highly efficient devices.

Acknowledgements

I would like to thank all the people who helped making the last year the special experience that it has been. Thanks to the people that said they want to meet again regardless of the place, to the ones who have been waiting for me to come back, and to the few who actually said they missed me. Thanks to both my Japanese supervisors, for the endless help they provided during this research, and thanks to my Italian supervisor, who kept reassuring saying that there is nothing wrong with a non-working thesis project. Thanks to my parents, for the financial help and for still wanting me to come back somehow.

Lastly, and most importantly, thanks to my two self-proclaimed favourite people in the world.

I don't even need to say why.

References

- [1] Coddington, O., J. L. Lean, P. Pilewskie, M. Snow, and D. Lindholm. "A Solar Irradiance Climate Data Record", *Bulletin of the American Meteorological Society* 97, 7 (2016): 1265-1282
- [2] Cui, Y.; Yao, H. F.; Zhang, J. Q.; Zhang, T.; Wang, Y. M.; Hong, L.; Xian, K. H.; Xu, B. W.; Zhang, S. Q.; Peng, J.; Wei, Z. X.; Gao, F.; Hou, J. H. Over 16% efficiency organic photovoltaic cells enabled by a chlorinated acceptor with increased open-circuit voltages. *Nat. Commun.* 2019, 10, 2515
- [3] Chen, Lin X. "Organic Solar Cells: Recent Progress and Challenges." *ACS energy letters* 4, no. 10 (2019): 2537–2539.
- [4] Gill, R. E., Hadziioannou, G., Lang, P., Garnier, F. & Wittmann, J. C. Highly oriented thin films of a substituted oligo(paraphenylenevinylene) on friction-transferred PTFE substrates. *Adv. Mater.* 9, 331–334 (1997)
- [5] Nagamatsu, S. et al. Multi-Layered Oriented Polyfuorene Films. *J. Phys. Chem. B* 113, 5746–5751 (2009)
- [6] Yoshida, Y., Tanigaki, N., Yase, K. & Hotta, S. Color-Tunable Highly Polarized Emissions from Uniaxially Aligned Tin Films of Thiophene/Phenylene Co-oligomers. *Adv. Mater.* 12, 1587–1591 (2000)
- [7] Sun, Sam-shajing. *Organic Photovoltaics: Mechanism, Materials and Devices*. Boca Raton: Taylor & Francis, 2005.
- [8] Sun, Sam-shajing. *Organic Photovoltaics: Mechanism, Materials and Devices – Chapter 5: Simulations of Optical Processes in Organic Photovoltaic Devices*. Boca Raton: Taylor & Francis, 2005.
- [9] Sun, Sam-shajing. *Organic Photovoltaics: Mechanism, Materials and Devices – Chapter 8: Optimization of Organic Solar Cells in Both Space and Energy–Time Domains*. Boca Raton: Taylor & Francis, 2005.
- [10] Sun, Sam-shajing. *Organic Photovoltaics: Mechanism, Materials and Devices – Chapter 9: Bulk Heterojunction Solar Cells*. Boca Raton: Taylor & Francis, 2005.
- [11] Fujii, Akihiko, Tomoki Shirakawa, Tokiyoshi Umeda, Hiroyoshi Mizukami, Yuuki Hashimoto, and Katsumi Yoshino. "Interpenetrating Interface in Organic Photovoltaic Cells with Heterojunction of Poly(3-Hexylthiophene) and C 60." *Japanese Journal of Applied Physics* 43, no. 8R (2004): 5573–.
- [12] Fujii, A, H Mizukami, Y Hashimoto, T Umeda, Y Nishihara, M Ozaki, And K Yoshino. "Highly Efficient Photovoltaic Cells Composed of Interpenetrating Conducting polymer/C60 Heterojunction." *Synthetic metals* 152, no. 1-3 (2005): 121–124.
- [13] Sun, Sam-shajing. *Organic Photovoltaics: Mechanism, Materials and Devices – Chapter 4: Solid state organic photovoltaics: a review of molecular and polymeric devices*. Boca Raton: Taylor & Francis, 2005.
- [14] Grell, Martin, Wolfgang Knoll, Donald Lupo, Andreas Meisel, Tzenka Miteva, Dieter Neher, Heinz-Georg Nothofer, Ullrich Scherf, and Akio Yasuda. "Blue Polarized Electroluminescence from a Liquid Crystalline Polyfluorene." *Advanced materials (Weinheim)* 11, no. 8 (1999): 671–675.
- [15] Cimrová, V., Remmers, M., Neher, D. and Wegner, G. (1996), Polarized light emission from LEDs prepared by the Langmuir-Blodgett technique. *Adv. Mater.*, 8: 146-149.
- [16] Makinson, K.R.; Tabor, D. The Friction and Transfer of Polytetrafluoroethylene. *Nature* 1964, 201, 464–466.
- [17] Wittmann, J., Smith, P. Highly oriented thin films of poly(tetrafluoroethylene) as a substrate for oriented growth of materials. *Nature* 352, 414–417 (1991).
- [18] Tanigaki, N.; Takechi, C.; Nagamatsu, S.; Mizokuro, T.; Yoshida, Y. Oriented Thin Films of Insoluble Polythiophene Prepared by the Friction Transfer Technique. *Polymers* 2021, 13, 2393.

- [19] Mizokuro, Toshiko, Keisuke Takeuchi, Claire Heck, Hiroyuki Aota, and Nobutaka Tanigaki. "Orientation Management of α -Sexithiophene Layer for the Application in Organic Photovoltaic Devices." *Organic electronics* 13, no. 12 (2012): 3130–3137.
- [20] Mizokuro, Toshiko, Claire Heck, and Nobutaka Tanigaki. "Orientation of α -Sexithiophene on Friction-Transferred Polythiophene Film." *The journal of physical chemistry. B* 116, no. 1 (2012): 189–193.
- [21] Hotta, Shu, Midori Goto, Reiko Azumi, Masamitsu Inoue, Musubu Ichikawa, and Yoshio Taniguchi. "Crystal Structures of Thiophene/Phenylene Co-Oligomers with Different Molecular Shapes." *Chemistry of materials* 16, no. 2 (2004): 237–241.
- [22] Inada, Yuhi, Masashi Koda, Yuji Urabe, Toshifumi Katagiri, Takeshi Yamao, Yuji Yoshida, and Shu Hotta. "Microcrystalline Array Structures Induced by Heat Treatment of Friction-Transferred Organic Semiconductor Films." *Scientific reports* 9, no. 1 (2019): 9739–11.
- [23] Kumari, Nikita, Manish Pandey, Shuichi Nagamatsu, Masakazu Nakamura, and Shyam S Pandey. "Investigation and Control of Charge Transport Anisotropy in Highly Oriented Friction-Transferred Polythiophene Thin Films." *ACS applied materials & interfaces* 12, no. 10 (2020): 11876–11883.
- [24] Mizokuro, Toshiko, Yukiyasu Okamoto, Claire Heck, Hiroyuki Aota, and Nobutaka Tanigaki. "Orientation Control of Regioregular-Poly(3-Dodecylthiophene) Films Formed by the Friction-Transfer Method and the Performance of Organic Photovoltaic Devices Based on These Films." *Journal of applied polymer science* 131, no. 8 (2014): np–n/a.
- [25] Mizokuro, Toshiko, Keisuke Takeuchi, Claire Heck, Hiroyuki Aota, and Nobutaka Tanigaki. "Orientation Management of α -Sexithiophene Layer for the Application in Organic Photovoltaic Devices." *Organic electronics* 13, no. 12 (2012): 3130–3137.
- [26] Osaka, Itaru, Toru Abe, Masafumi Shimawaki, Tomoyuki Koganezawa, and Kazuo Takimiya. "Naphthodithiophene-Based Donor–Acceptor Polymers: Versatile Semiconductors for OFETs and OPVs." *ACS macro letters* 1, no. 4 (2012): 437–440.
- [27] Videlot, C., and D. Fichou. "Influence of Molecular Orientation on the Photovoltaic Properties of Octithiophene." *Synthetic metals* 102, no. 1 (1999): 885–888.
- [28] Videlot, C, A El Kassmi, and D Fichou. "Photovoltaic Properties of Octithiophene-Based Schottky and P/n Junction Cells: Influence of Molecular Orientation." *Solar energy materials and solar cells* 63, no. 1 (2000): 69–82.
- [29] Taniguchi, Tomoki, Kenichiro Fukui, Ryo Asahi, Yuji Urabe, Akito Ikemoto, Junki Nakamoto, Yuhi Inada, Takeshi Yamao, and Shu Hotta. "Enhanced Performance of Organic Solar Cells Based on Thiophene/phenylene Co-Oligomers." *Synthetic metals* 227 (2017): 156–162.
- [30] Destruel, Pierre, Harald Bock, Isabelle Séguy, Pascale Jolinat, Mimoun Oukachmih, and Elena Bedel-Pereira. "Influence of Indium Tin Oxide Treatment Using UV-Ozone and Argon Plasma on the Photovoltaic Parameters of Devices Based on Organic Discotic Materials." *Polymer international* 55, no. 6 (2006): 601–607.
- [31] Sugiyama, Kiyoshi, Hisao Ishii, Yukio Ouchi, and Kazuhiko Seki. "Dependence of Indium–tin–oxide Work Function on Surface Cleaning Method as Studied by Ultraviolet and x-Ray Photoemission Spectroscopies." *Journal of applied physics* 87, no. 1 (2000): 295–298.

